Supporting information

Quantification of thermodynamic effects of carbohydrate multivalency on avidity using synthetic discrete glycooligomers

Masanori Nagao[a]*, Yu Hoshino[b]* and Yoshiko Miura[a]*

[a]Department of Chemical Engineering, Kyushu University, 744 Motooka, Nishi-ku, Fukuoka 819-0395, Japan.
[b]Department of Applied Chemistry, Kyushu University, 744 Motooka, Nishi-ku, Fukuoka 819-0395, Japan.

E-mail: nagaom@chem-eng.kyushu-u.ac.jp

Table of Contents

1. Materials and Methods

2,2'-Azobis(isobutyronitrile) (AIBN, 98%), acetic acid, calcium chloride, manganese chloride tetrahydrate, sodium methoxide (95%), and phosphate-buffered saline (PBS) were purchased from FUJIFILM Wako Pure Chemical Co. (Tokyo, Japan). 2,5-Dihydroxybenzoic acid (DHBA) was purchased from Tokyo Chemical Industry Co. (Tokyo, Japan). Maleimide-functionalized polyethylene glycols with molecular weights of 3.4 kDa, 6 kDa, and 10 kDa (Mal-PEG-Mal) were purchased from Funakoshi Co. (Tokyo, Japan). *N*,*N*-Dimethylformamide (DMF), methanol, sodium acetate, and sodium chloride were purchased from Kanto Chemical (Tokyo, Japan). 2-Cyano-2-propyl dodecyl trithiocarbonate (CPDTC), tris(2-carboxyethyl)phosphine hydrochloride (TCEP), and concanavalin A (ConA, powder) were purchased from Sigma-Aldrich Co. (MO, US). Mannose acrylamide (ManAAm) and glucose acrylamide (GlcAAm) were prepared according to previous papers.[1,2] AIBN was purified by recrystallization from methanol prior to use. Water used in this experiment was prepared using a Direct-Q Ultrapure Water System (Merck, Limited).

Proton nuclear resonance (^{1}H NMR) spectra were recorded on a JEOL-ECP400 spectrometer (JEOL, Tokyo, Japan) using DMSO-d_6 or D_2O. Automated flash column chromatography was performed on a Biotage Isolera One ISO-1SW equipment, equipped with a Biotage SNAP Ultra C18 column cartridge (30 g/ 120 g); elution was performed with water and MeOH. For ultra-performance liquid chromatography-mass spectrometry (UPLC-MS), an ACQUITY Sample Manager FTN-H (Waters, Waters Corporation, Massachusetts, USA), ACQUITY Quaternary Solvent Manager (Waters), ACQUITY Column Manager (Waters), PDA eλ Detector (Waters), and ACQUITY QDA detector (Waters) were used. The data were analyzed by using Empower SOFTWARE (Waters). To analyze the oligomers, the samples were dissolved in methanol (containing 0.1% formic acid) and analyzed by UPLC-MS at room temperature. Detection was performed using an ACQUITY QDA detector (ionization mode: ESI positive). Matrix assisted laser desorption ionization time of flight (MALDI-TOF) MS was recorded in linear mode on a Bruker Autoflex III MALDI-ToF mass spectrometer. The polymer solution and the matrix solution were prepared by dissolving polymer analytes (50 μg/mL) or DHBA (10 mg/mL) in a mixture of acetonitrile and 0.1 v/v% TFA (aq) (2: 1), respectively. Mixture of the polymer solution and matrix solution (1: 1) was put on a stainless steel MALDI plate (1 μL of the mixture), and the solvent was dried at room temperature. Size exclusion chromatography (SEC) analyses with water solvent was performed on a JASCO DG-980-50 degasser equipped with a JASCO PU-980 pump (JASCO Co., Tokyo, Japan), a Superdex 200 Increase 10/300 GL column (Cytiva, U.S.), a JASCO RI-2031 Plus RI detector. The analysis was performed at a flow rate of 0.5 mL/min by injecting 20 μL of a polymer solution (2 g/L) in 100 mM $NaNO_3$ aqueous solution (20 °C). All the samples were previously filtered through a 0.22 μm filter. The SEC system was calibrated using a polyethylene glycol standard.

2. Synthesis of discrete glycooligomers

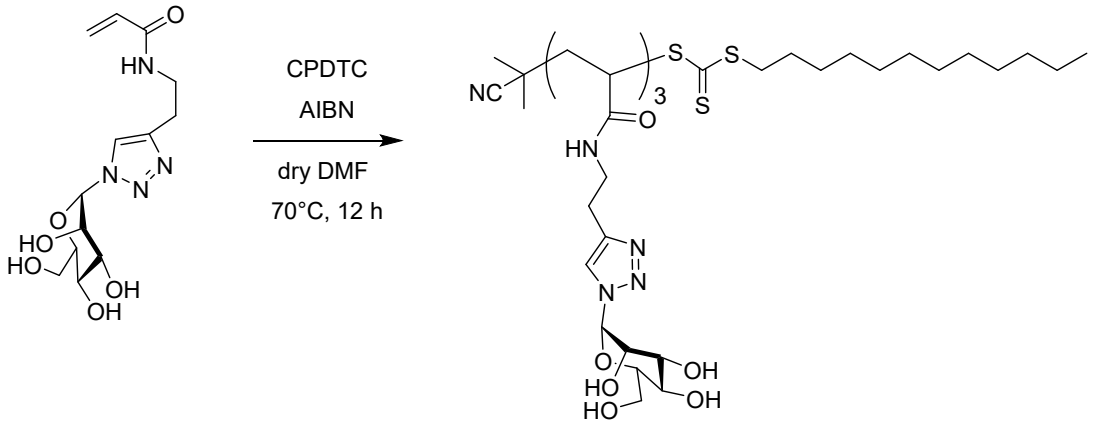

ManAAm (150 mg, 0.46 mmol) was dissolved in dry DMF (900 μL) with CPDTC (53 mg, 0.15 mmol) and AIBN (5 mg, 0.030 mmol). The solution was degassed by freeze-thaw cycles (three times) and placed in an oil bath. The reaction proceeded at 70 °C for 12 hours. The reaction was stopped by exposing it to air. The conversion was determined by ^{1}H NMR using DMSO-d_6 (Figure S1). The DMF solvent was removed under reduced pressure, and 1 mL of methanol was added. The obtained glycooligomers in the solution was separated by the reverse-phase chromatography (Figure S2). The fractions were collected and concentrated under reduced pressure. The fractionated glycooligomers were obtained as yellow powders after freeze-drying. While the glycooligomer with DP of 1 (**M1**) did not dissolve in water, the suspension in water was freeze-dried. The structures of the glycooligomers were analyzed by ^{1}H NMR, UPLC-MS, and MALDI-TOF MS (Figure S3, S4, and S5).

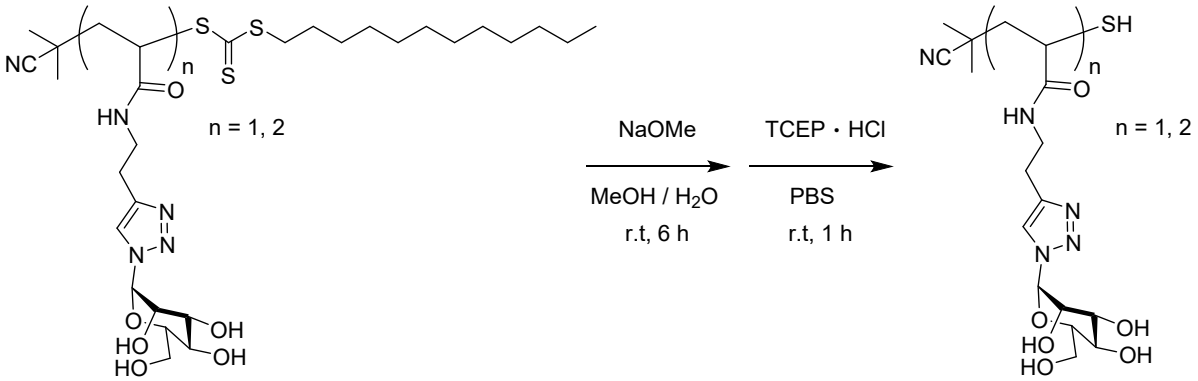

The RAFT terminals of the glycooligomers were converted to thiol group by hydrolysis. The glycooligomer (40 mg) was dissolved in a mixture of methanol (2 mL) and water (200 μL) with sodium methoxide (25 mg). The solution was kept stirring at room temperature for 6 hours. The methanol solvent was removed under reduced pressure, and 1 mL of PBS was added with 2 mg of TCEP. After 1 hour, the glycooligomer with thiol terminal was purified by the reverse-phase chromatography. The objective was obtained as white powder after freeze-drying. The structures of the glycooligomers with thiol terminal were analyzed by ^{1}H NMR and UPLC-MS (Figure S6 and S7).

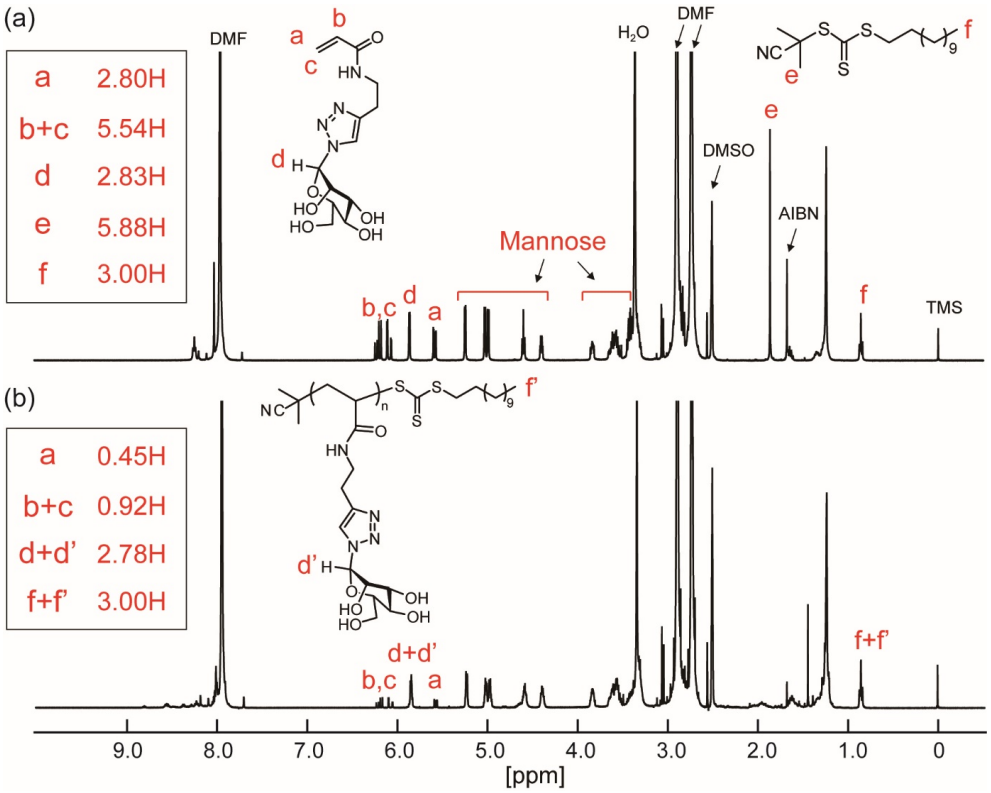

Figure S1. ^{1}H NMR spectra of polymerization solution before (a) and after (b) the reaction.

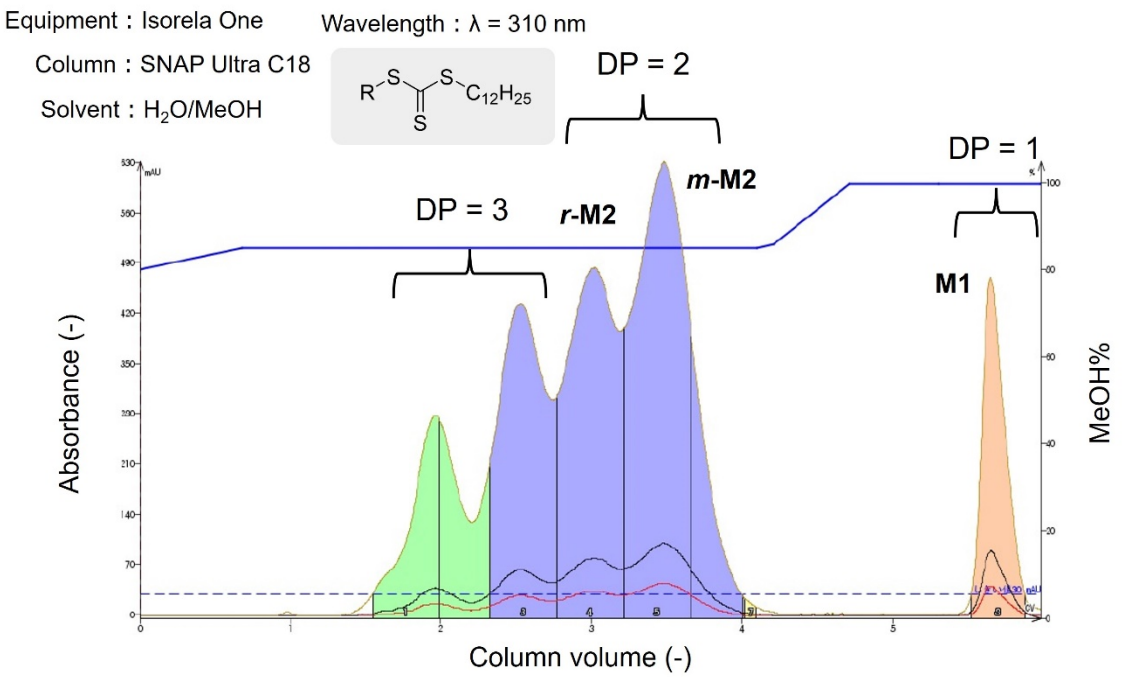

Figure S2. Chromatogram for isolation of the glycooligomer mixture.

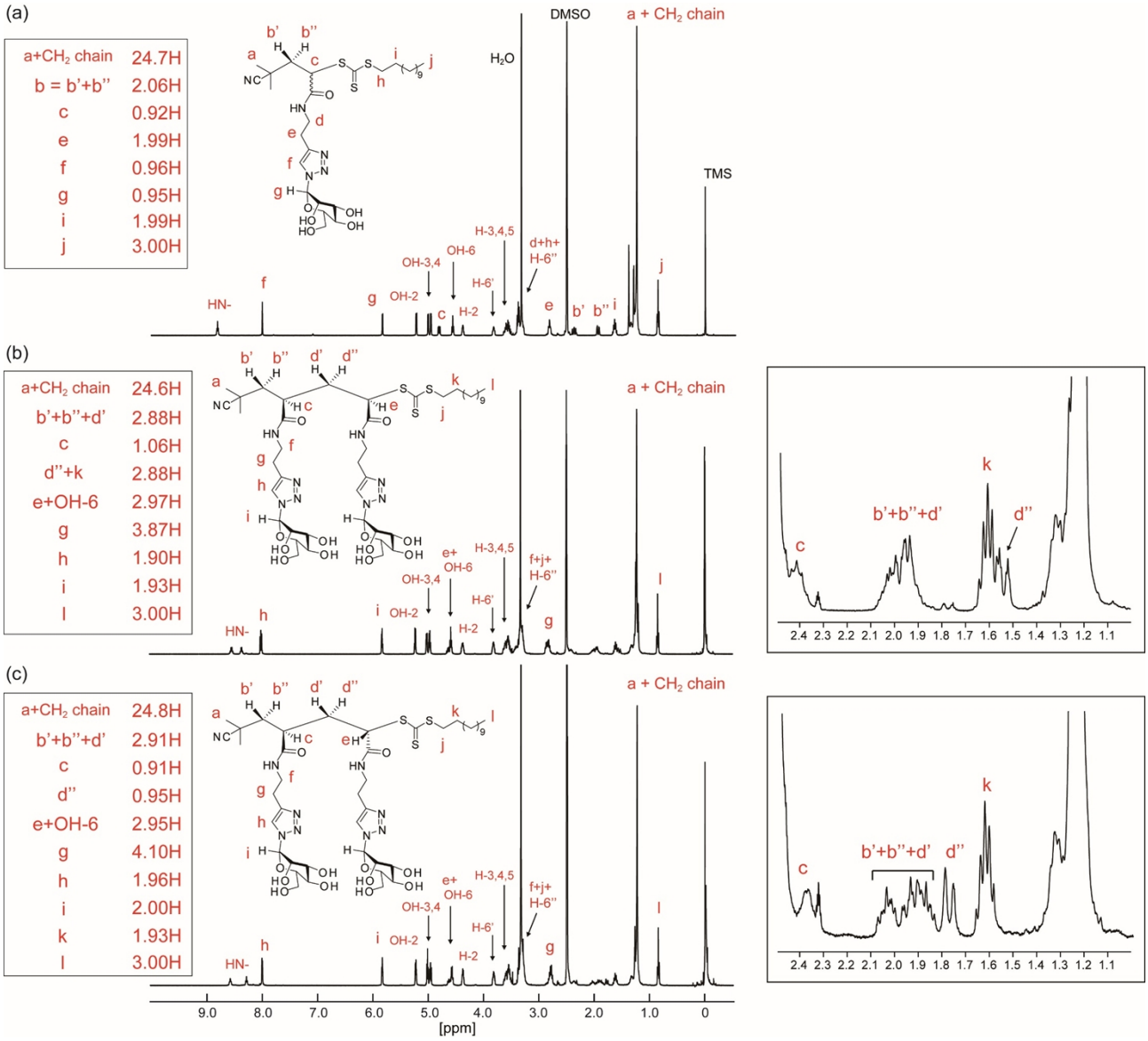

Figure S3. ^{1}H NMR spectra of the isolated glycooligomers. (a) **M1**, (b) ***m*-M2** (meso), and (c) ***r*-M2** (racemo), respectively.

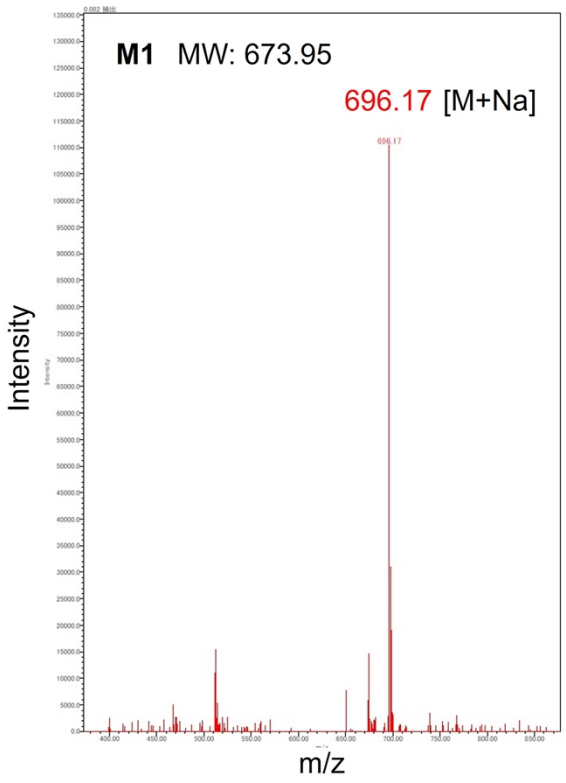

Figure S4. ESI-MS spectrum of **M1**. Theoretical value (m/z): [**M1**]+Na^+ = 696.94.

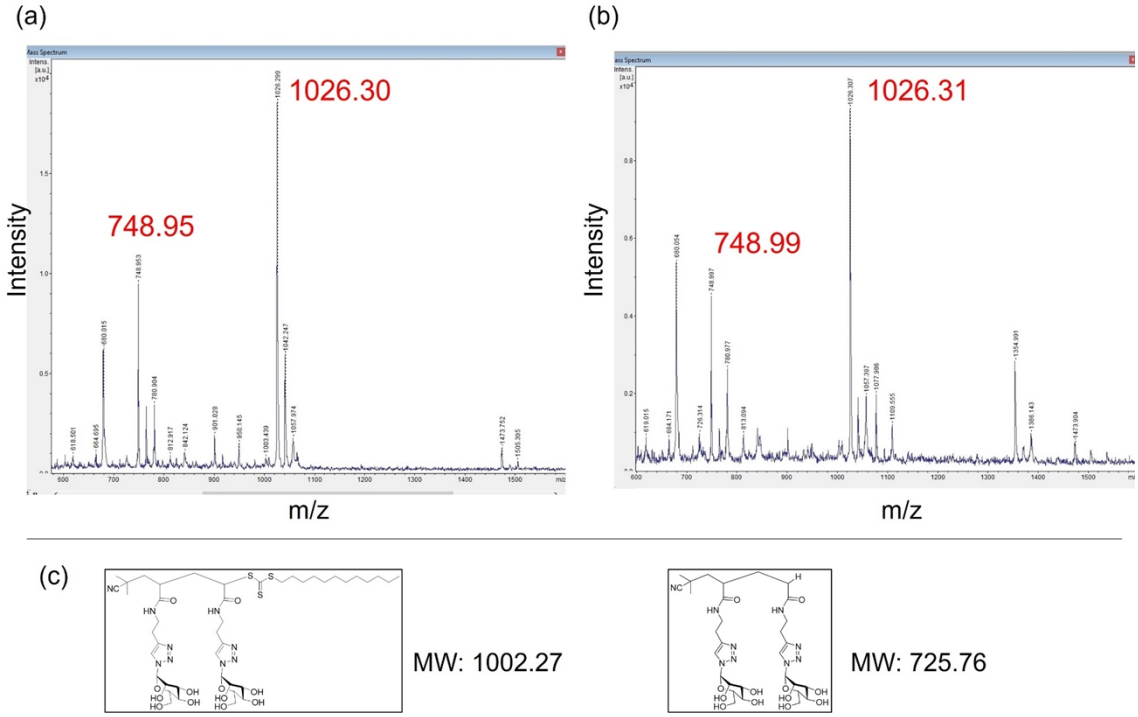

Figure S5. MALDI-TOF MS spectra of (a) ***m*-M2** and (b) ***r*-M2**, and molecular weights for each fractioned structure (c). Theoretical value (m/z): [**M2**]+Na^+ = 1025.26, [**M2**−RAFT terminal]+Na^+ = 748.75.

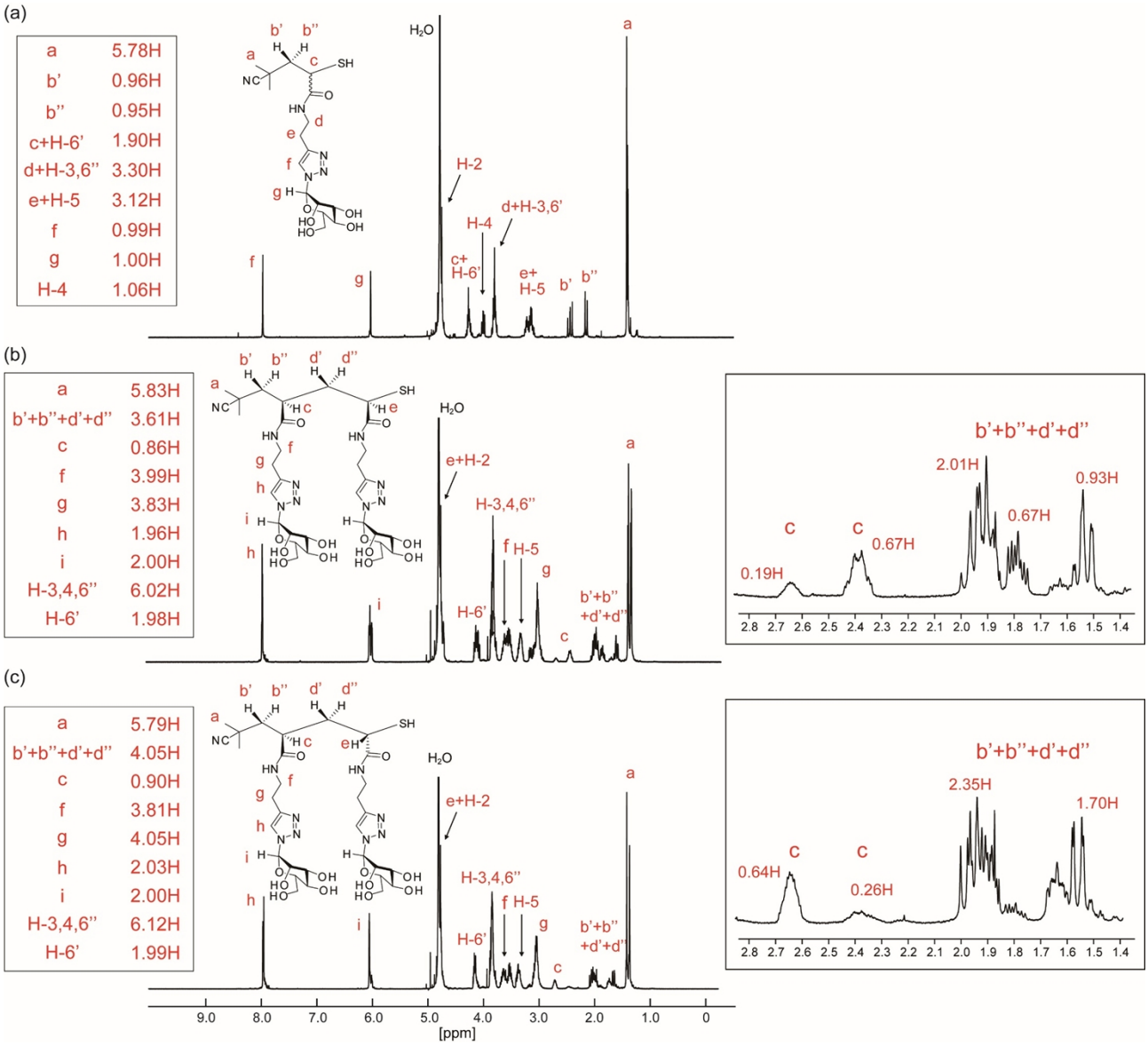

Figure S6. ^{1}H NMR spectra of the glycooligomers with thiol terminal. (a) **M1-SH**, (b) ***m*-M2-SH** (meso), and (c) ***r*-M2-SH** (racemo), respectively.

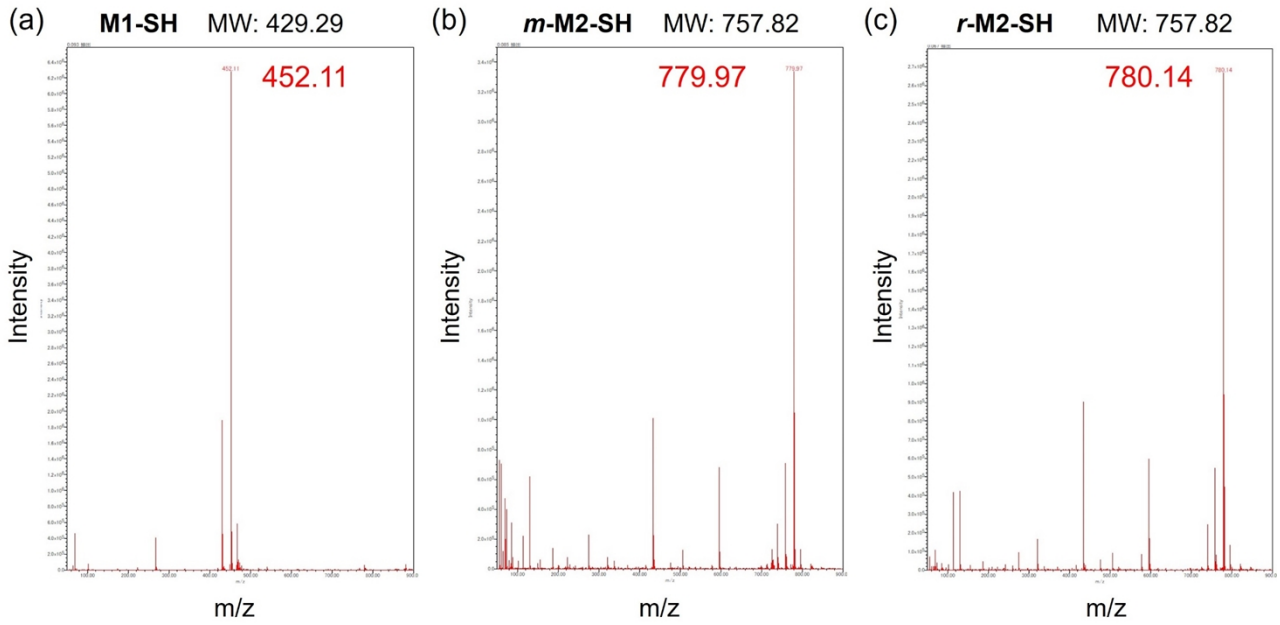

Figure S7. ESI-MS spectra of **M1-SH**, ***m*-M2-SH**, and ***r*-M2-SH**.
Theoretical value (m/z): [**M1-SH**]+Na^+ = 452.28, [**M2-SH**]+Na^+ = 780.81.

3. Synthesis of divalent glycoligands with PEG linkers

To Mal-PEG-Mal in a vial, the glycooligomer solution in PBS (2 mL) was added. The concentration of the glycooligomers was prepared to be 2 eq to the molar amount of maleimide groups of Mal-PEG-Mal. The amounts of compounds are summarized in Table S1. The solution was kept stirring at room temperature for 6 hours. The glycoligands with PEG linkers were purified by dialysis against water (MWCO = 3,500), followed by freeze-drying. The structures of the glycoligands were analyzed by ^{1}H NMR, MALDI-TOF MS, and SEC.

Table S1. Detailed conditions and results for conjugation reaction of glycooligomers with PEG linkers.

	MW of PEG	Mal-PEG-Mal (molar amount of maleimide)	**M1-SH** (molar amount)	**M2-SH** (molar amount)	M_n (g/mol)	M_w (g/mol)	M_w/M_n
M1-PEG$_{3.4k}$-M1	3.4 kDa	20 mg (12 μmol)	11 mg (26 μmol)	- -	3,200	3,300	1.04
M2-PEG$_{3.4k}$-M2	3.4 kDa	20 mg (12 μmol)	- -	18 mg (24 μmol)	3,200	3,400	1.05
M1-PEG$_{6k}$-M1	6 kDa	30 mg (10 μmol)	8.5 mg (20 μmol)	- -	5,900	6,100	1.03
M2-PEG$_{6k}$-M2	6 kDa	30 mg (10 μmol)	- -	15 mg (20 μmol)	6,300	6,500	1.03
M1-PEG$_{10k}$-M1	10 kDa	20 mg (4 μmol)	4.5 mg (80 μmol)	- -	9,400	9,500	1.01
M2-PEG$_{10k}$-M2	10 kDa	20 mg (4 μmol)	- -	6 mg (8 μmol)	9,700	9,800	1.01

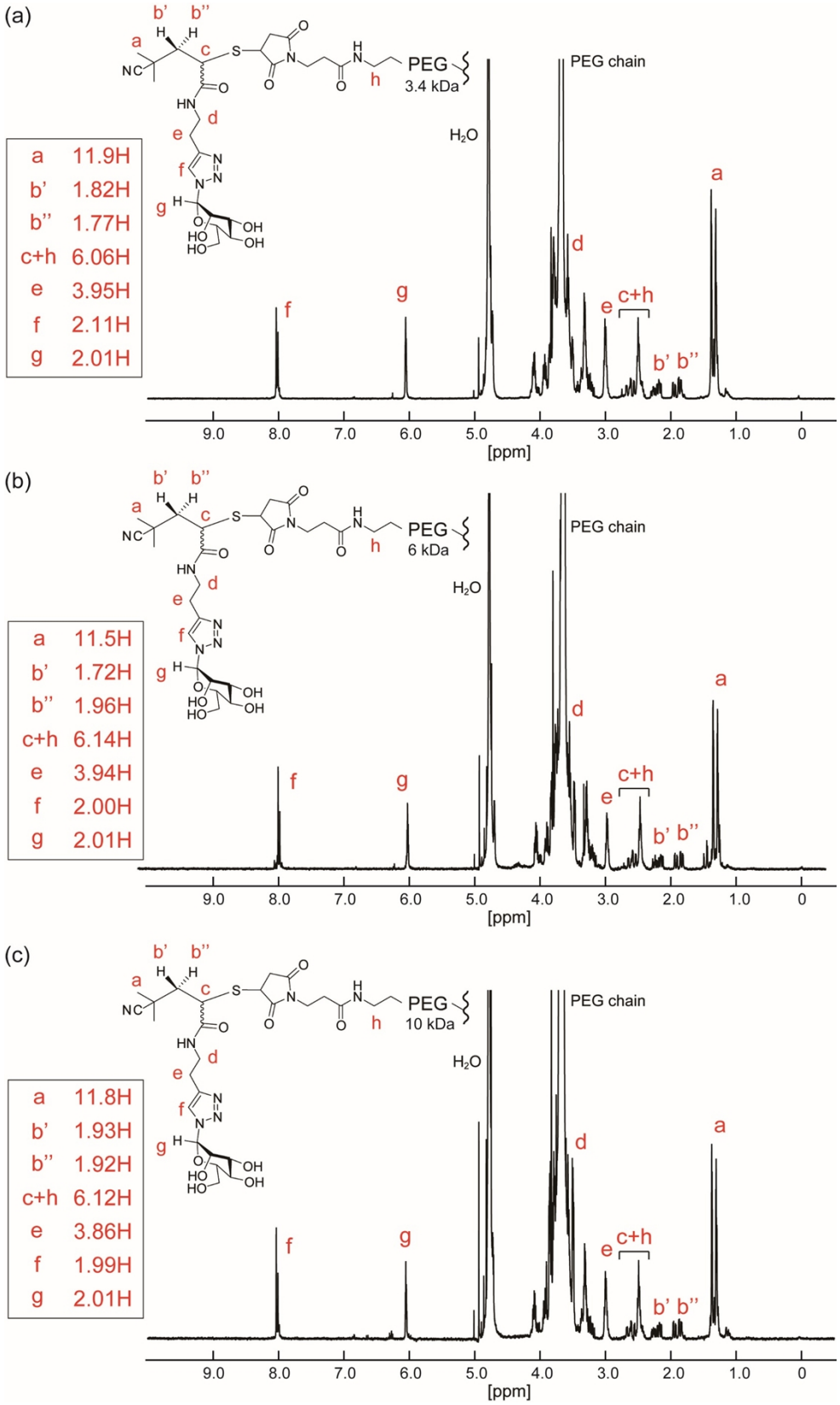

Figure S8. ^{1}H NMR spectra of divalent glycoligands with **M1**. The molecular weights of PEG linkers were 3.4 kDa (a), 6 kDa (b), and 10 kDa (c), respectively.

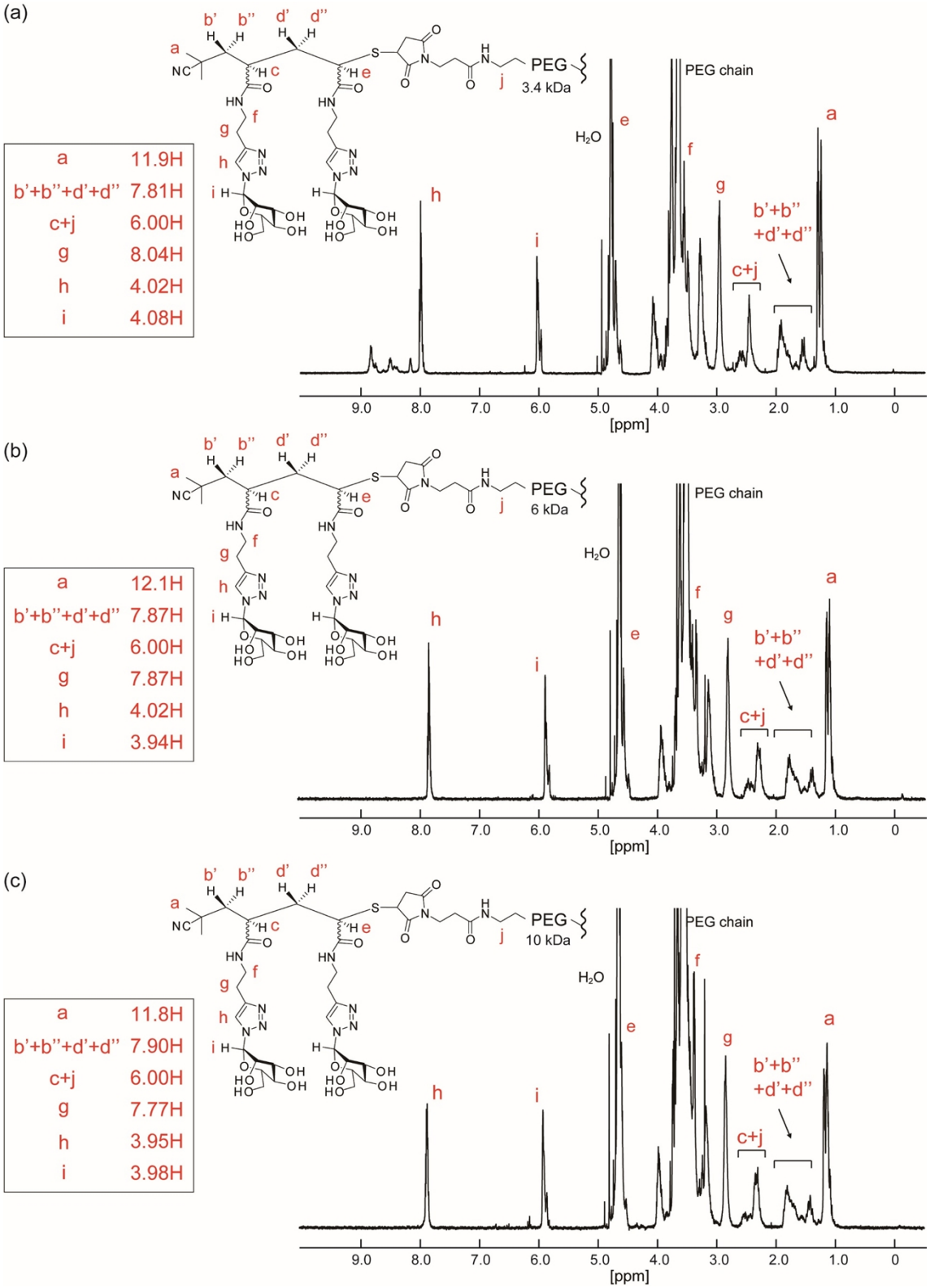

Figure S9. ^{1}H NMR spectra of divalent glycoligands with **M2**. The molecular weights of PEG linkers were 3.4 kDa (a), 6 kDa (b), and 10 kDa (c), respectively.

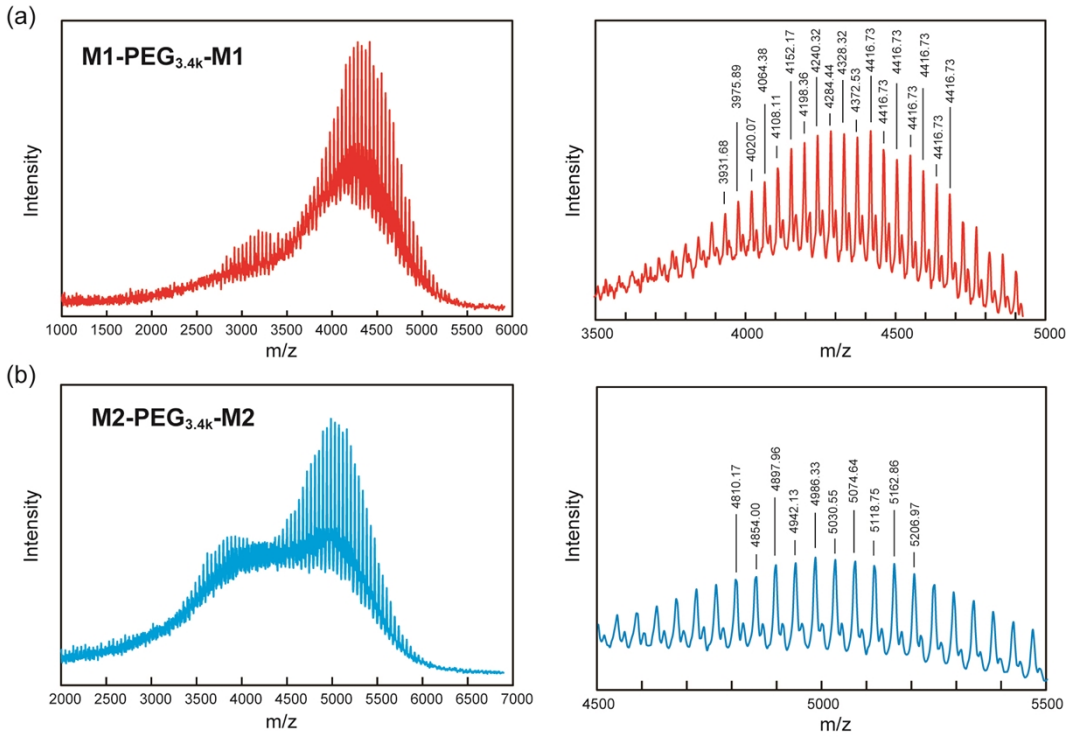

Figure S10. MALDI-TOF MS spectra of divalent glycoligands with PEG of 3.4 kDa.
(a) **M1-PEG$_{3.4k}$-M1** and (b) **M2-PEG$_{3.4k}$-M2**.

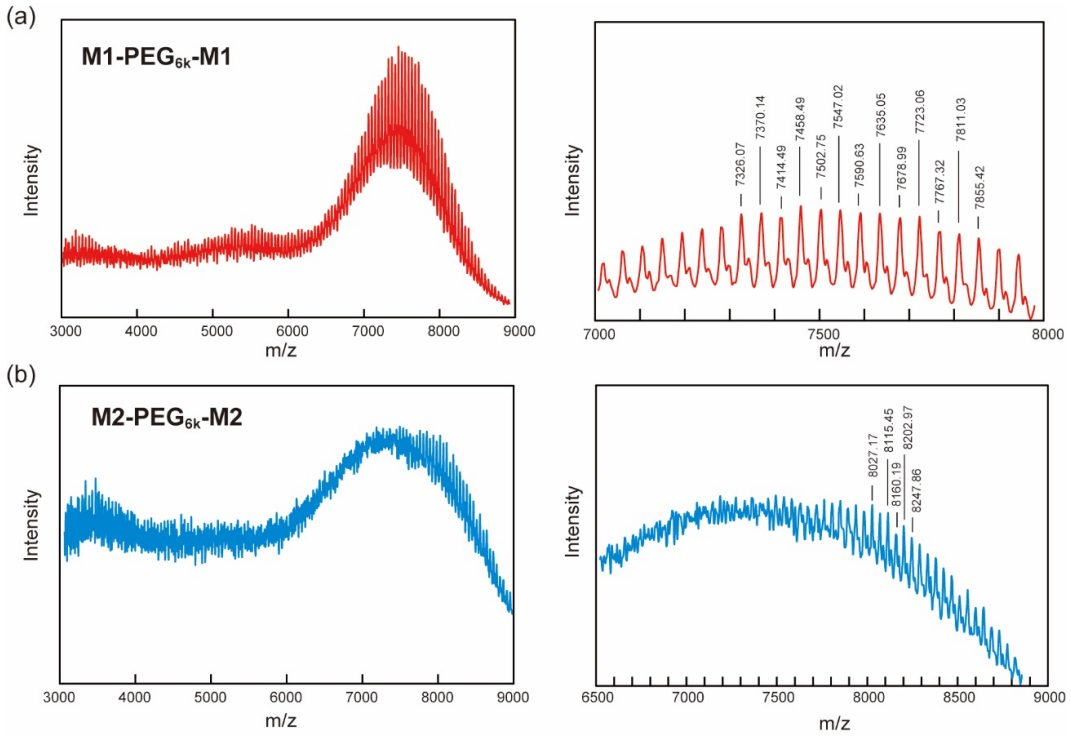

Figure S11. MALDI-TOF MS spectra of divalent glycoligands with PEG of 6 kDa.
(a) **M1-PEG$_{6k}$-M1** and (b) **M2-PEG$_{6k}$-M2**.

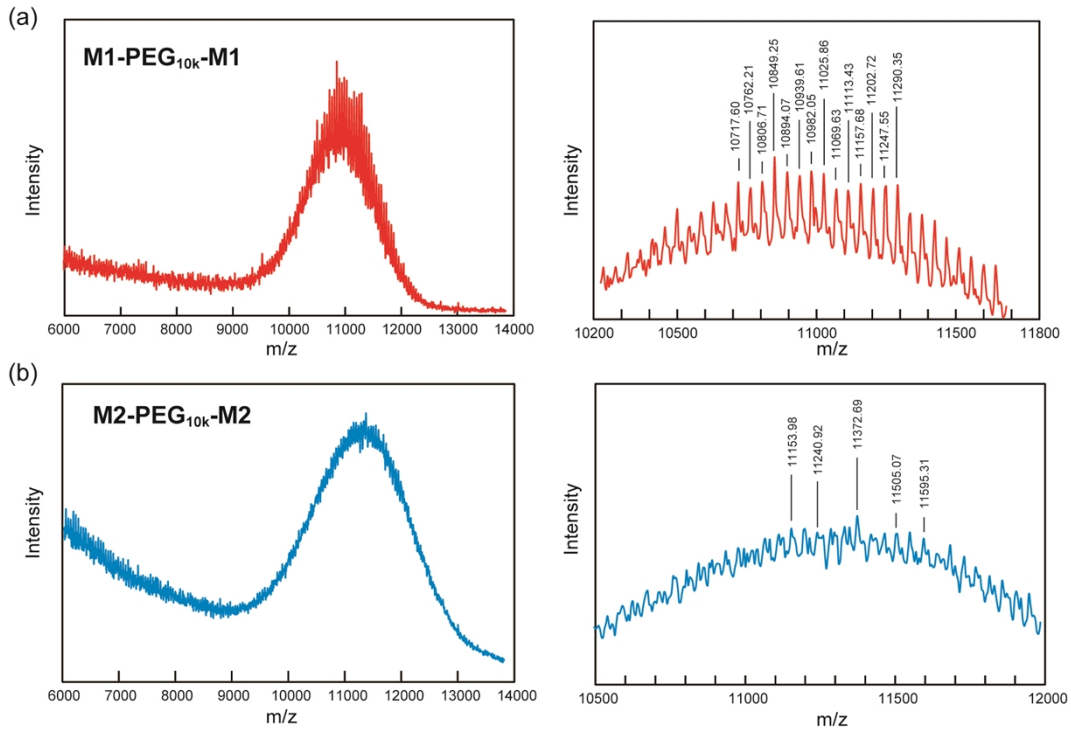

Figure S12. MALDI-TOF MS spectra of divalent glycoligands with PEG of 10 kDa. (a) **M1-PEG$_{10k}$-M1** and (b) **M2-PEG$_{10k}$-M2**.

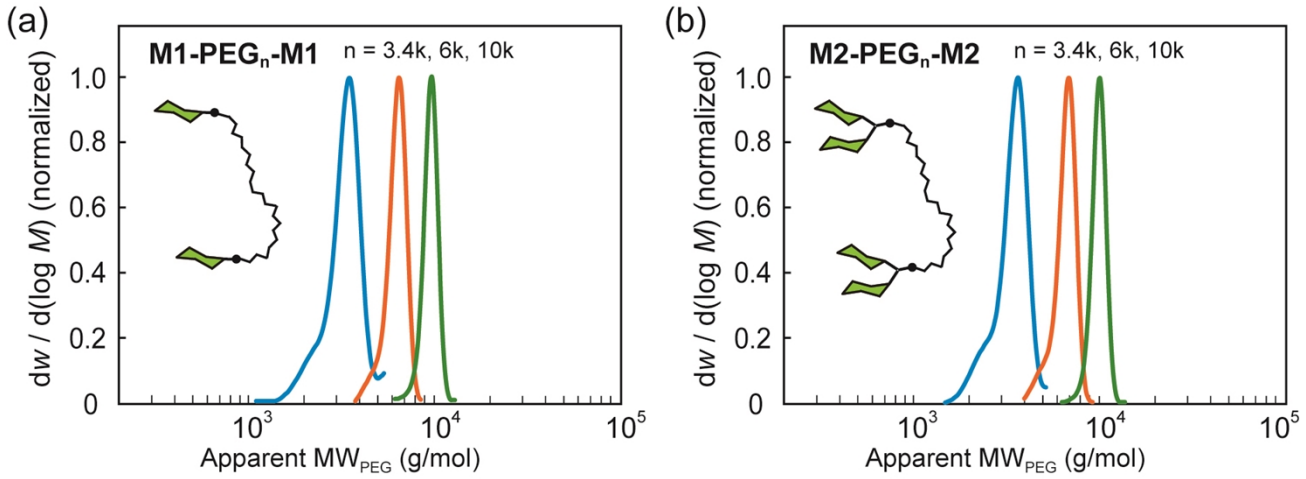

Figure S13. Molecular weight distributions of the divalent glycoligands with PEG linkers. (a) **M1-PEG$_n$-M1** and (b) **M2-PEG$_n$-M2**. Blue lines, orange lines and green lines represent the PEG molecule weight of 3.4k, 6k, and 10k, respectively. The eluent was water with 100 mM $NaNO_3$. The systems were calibrated with polyethylene glycol standards.

4. ITC measurements

All measurements of isothermal titration calorimetry (ITC) were performed by PEAQ-ITC (Malvern) in acetate buffer (2 mM acetic acid, 8 mM sodium acetate, 50 mM NaCl, 1 mM $CaCl_2$, and 1 mM $MnCl_2$, pH 5.2) with stirring at 750 rpm. The glycoligands were dissolved in the acetate buffer (2 ~ 5 mM), and the sample solutions were used without filtration. To prepare a ConA solution, ConA powder was dissolved in the acetate buffer (3 ~ 5 g/L), followed by filtration (0.22 μm filter). The accurate ConA concentration was determined spectrophotometrically on Agilent 8453 spectrophotometer at UV 280 nm using $A^{1\%,1cm} = 12.4$ for ConA at pH 5.2.[3] The Con A solution was placed in the cell and the glycoligand solutions were loaded into the syringe. The concentration of ConA dimer for each measurement was shown in Figure of raw data as [Cell]. During titration, 0.4μL was injected, followed by 18 injections of the same 2μL, each with a duration of 150s between each injection. Glycoligand to the buffer control titrations were subtracted from all experiments (in a point-by-point). The acquired data were fitted to a single-binding-stie model using the Microcal PEAQ-ITC Analysis software. The obtained binding data was not sigmoidal, indicating the weak interaction. To avoid overparameterization during fitting the data, the stoichiometry in the measurements of glycomonomers and glycooligomers were fixed to 2 owing to the two binding sites of ConA dimer. Similarly, the stoichiometry in the measurements of divalent glycoligands with PEG linkers were fixed to 1, assuming the multivalent binding.

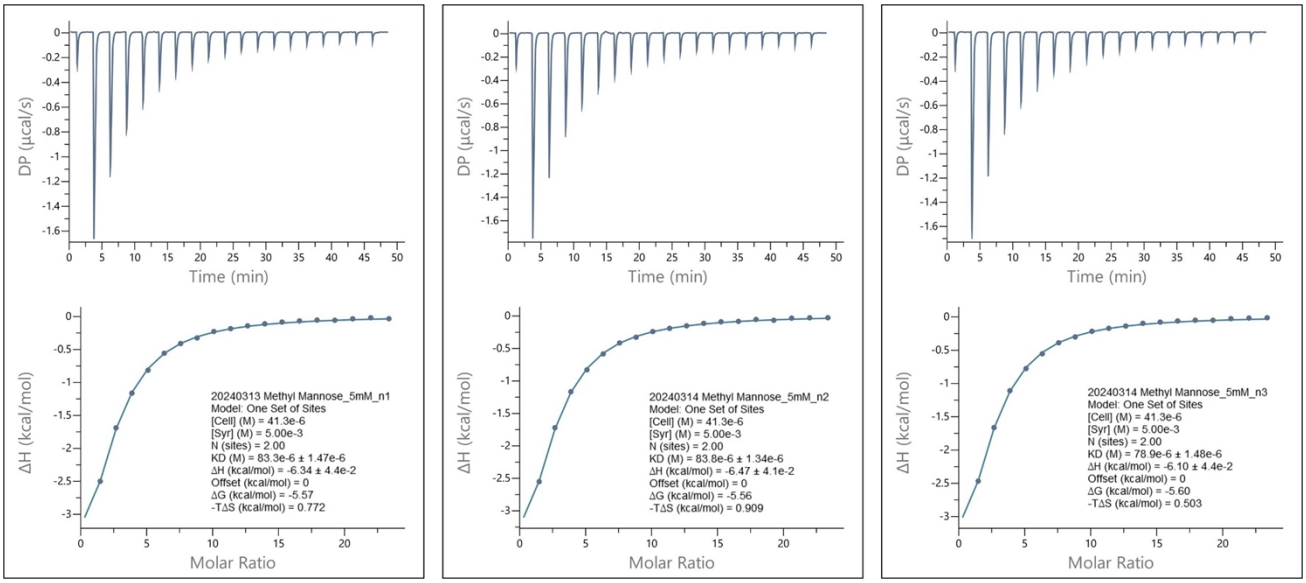

Figure S14. ITC data for the binding of methyl α-mannopyranoside to ConA at 25 ˚C. Raw thermograms after subtracting the control experiment at the top and binding isotherm (normalized heats versus molar ratio) at the bottom.

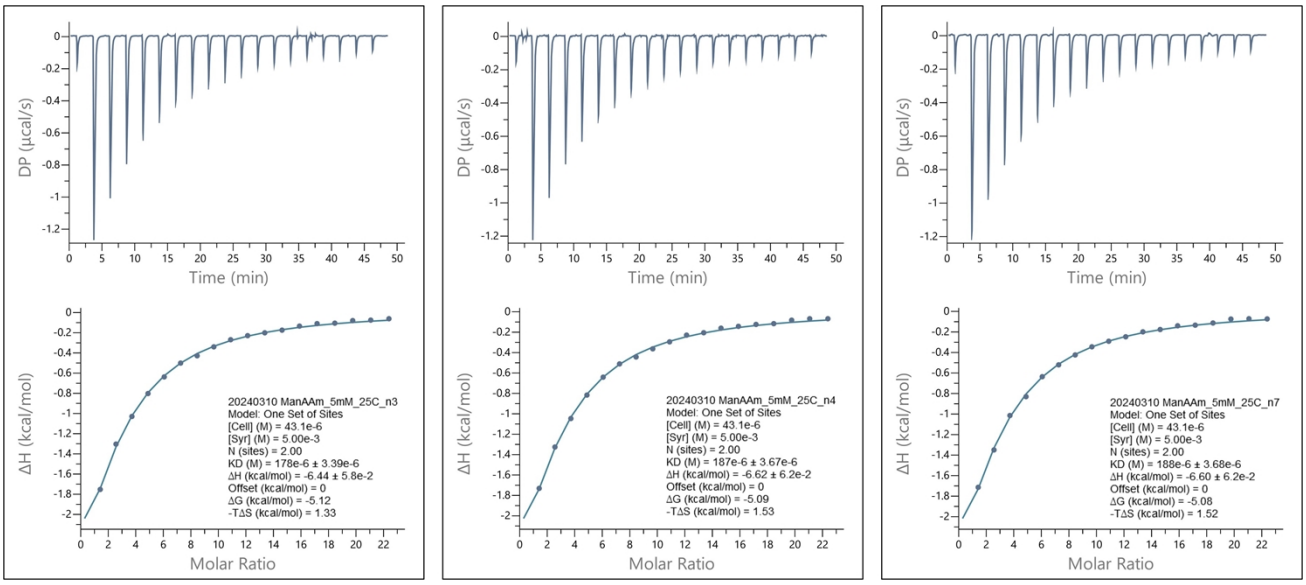

Figure S15. ITC data for the binding of ManAAm to ConA at 25 ˚C. Raw thermograms after subtracting the control experiment at the top and binding isotherm (normalized heats versus molar ratio) at the bottom.

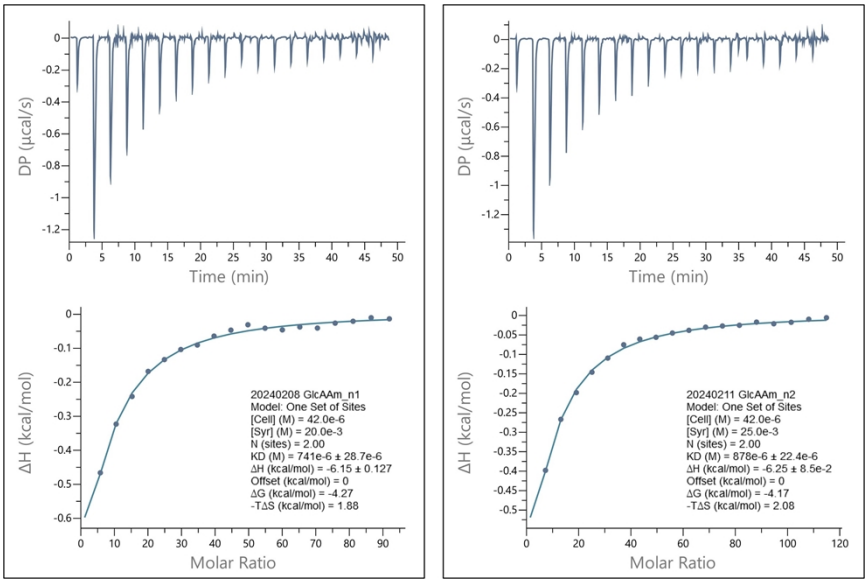

Figure S16. ITC data for the binding of GlcAAm to ConA at 25 ˚C. Raw thermograms after subtracting the control experiment at the top and binding isotherm (normalized heats versus molar ratio) at the bottom.

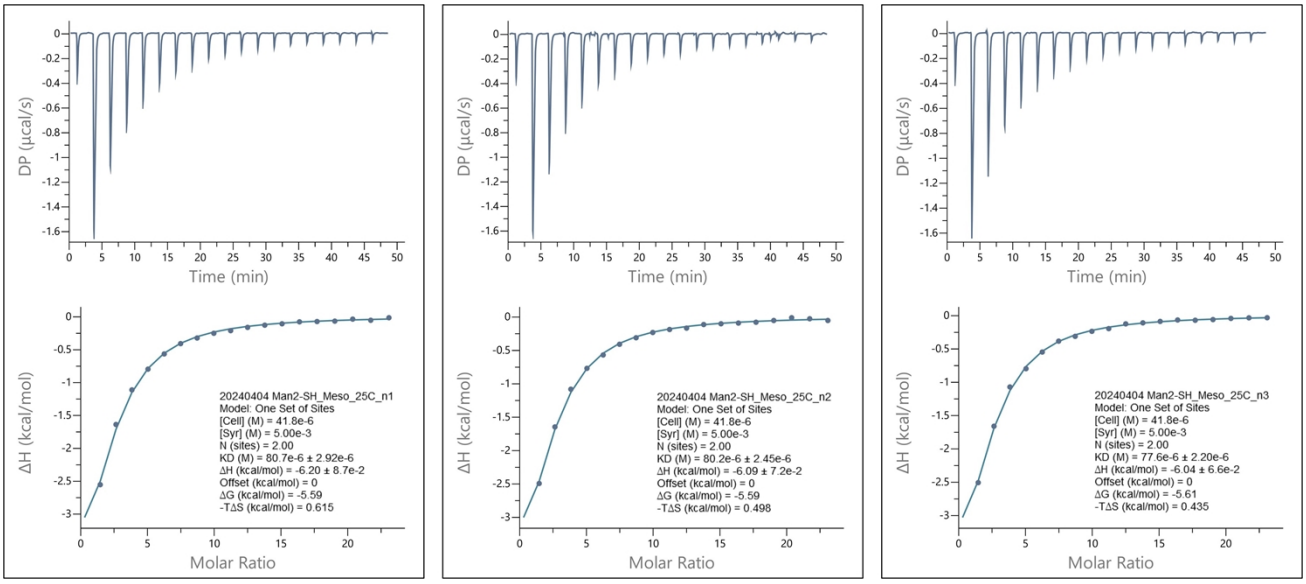

Figure S17. ITC data for the binding of ***m*-M2-SH** to ConA at 25 ˚C. Raw thermograms after subtracting the control experiment at the top and binding isotherm (normalized heats versus molar ratio) at the bottom.

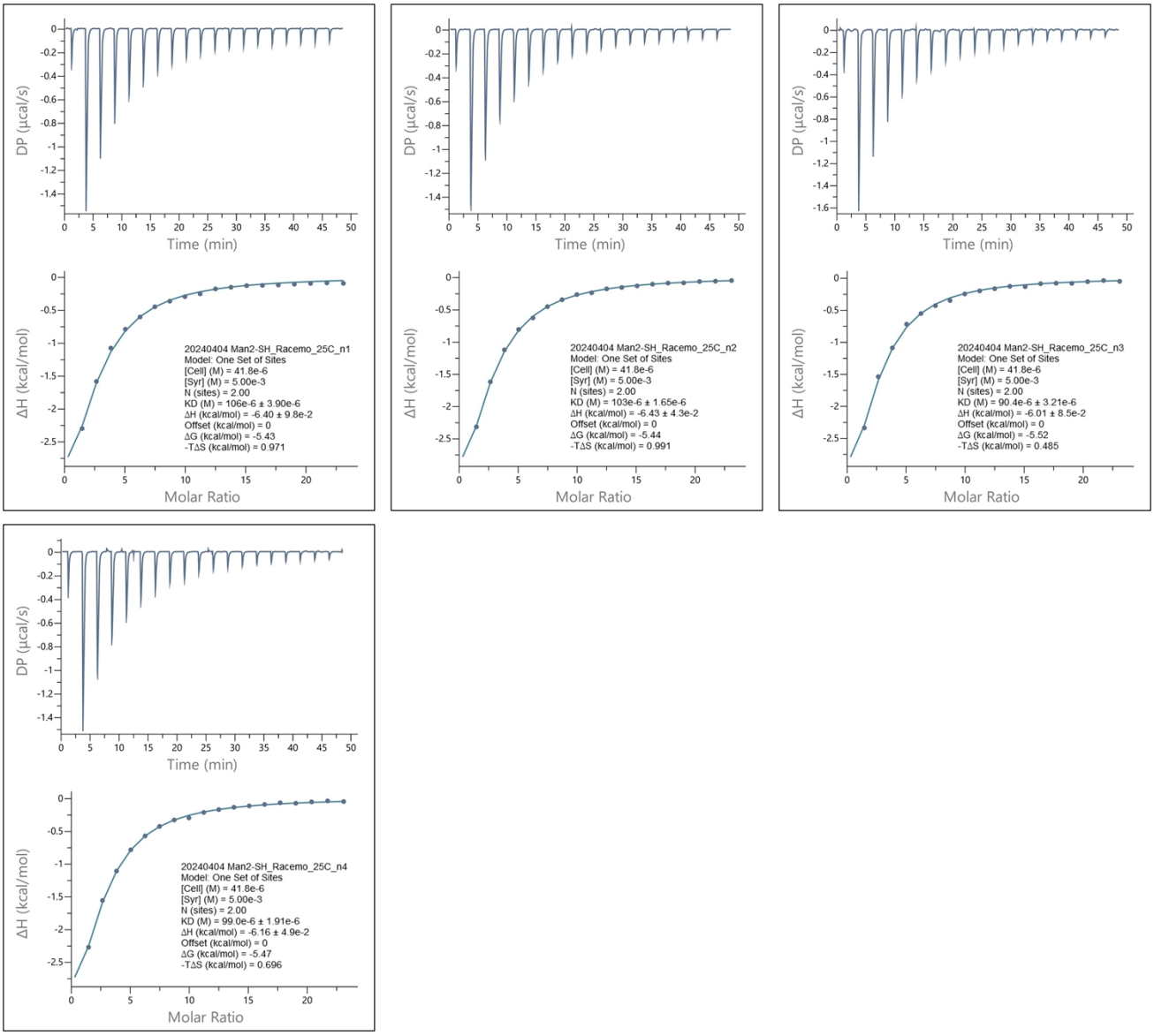

Figure S18. ITC data for the binding of ***r*-M2-SH** to ConA at 25 ˚C. Raw thermograms after subtracting the control experiment at the top and binding isotherm (normalized heats versus molar ratio) at the bottom.

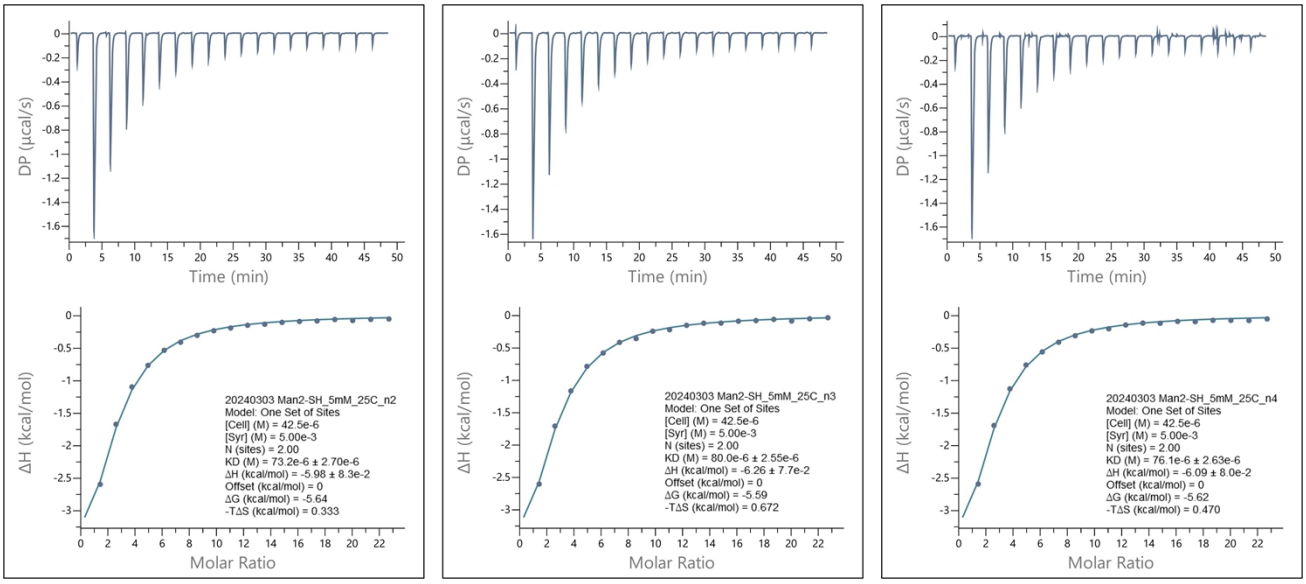

Figure S19. ITC data for the binding of **M2-SH** to ConA at 25 ˚C. Raw thermograms after subtracting the control experiment at the top and binding isotherm (normalized heats versus molar ratio) at the bottom.

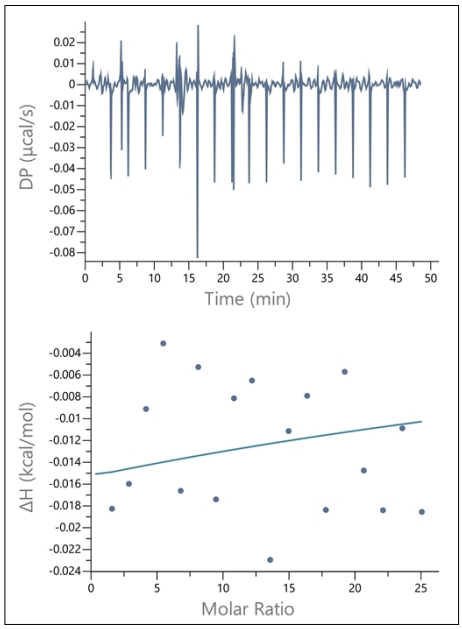

Figure S20. ITC data for the mixing of thioglycerol to ConA at 25 ˚C. Raw thermograms after subtracting the control experiment at the top and binding isotherm (normalized heats versus molar ratio) at the bottom. The concentrations of thioglycerol and ConA dimer were 5 mM and 39 µM,

respectively.

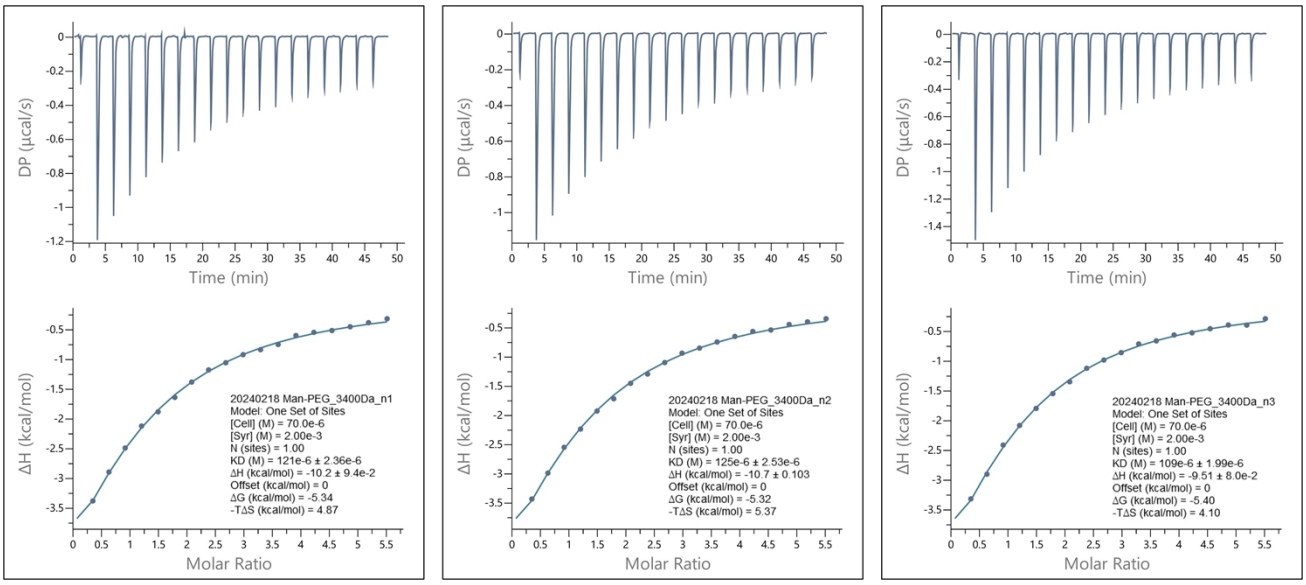

Figure S21. ITC data for the binding of **M1-PEG$_{3.4k}$-M1** to ConA at 25 ˚C. Raw thermograms after subtracting the control experiment at the top and binding isotherm (normalized heats versus molar ratio) at the bottom.

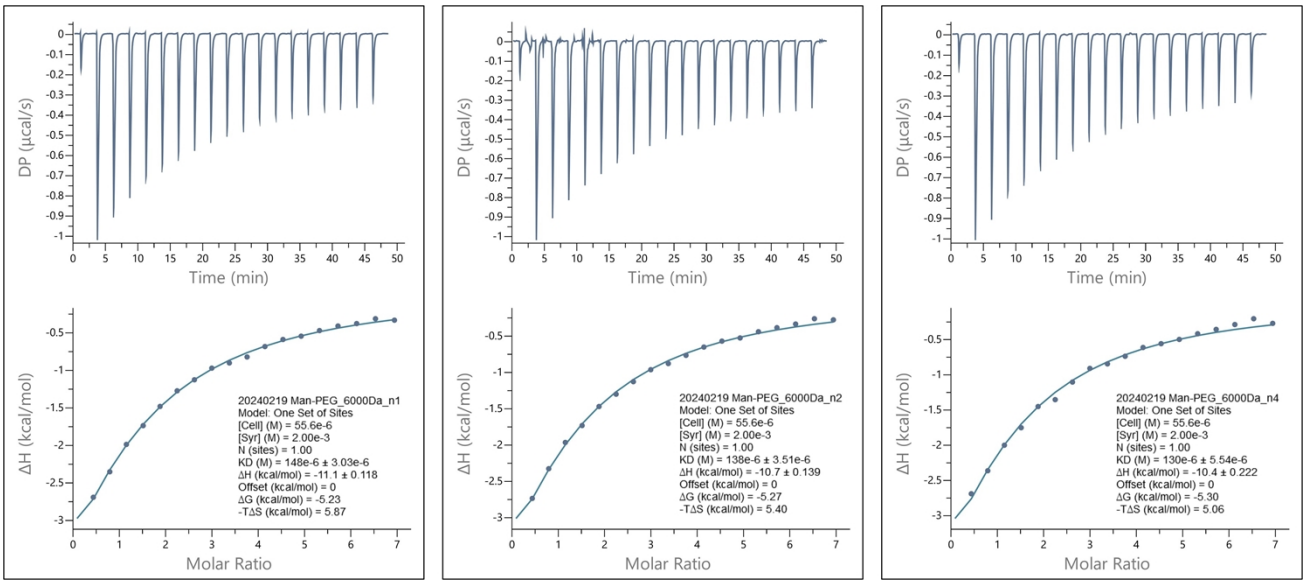

Figure S22. ITC data for the binding of **M1-PEG$_{6k}$-M1** to ConA at 25 ˚C. Raw thermograms after subtracting the control experiment at the top and binding isotherm (normalized heats versus molar ratio) at the bottom.

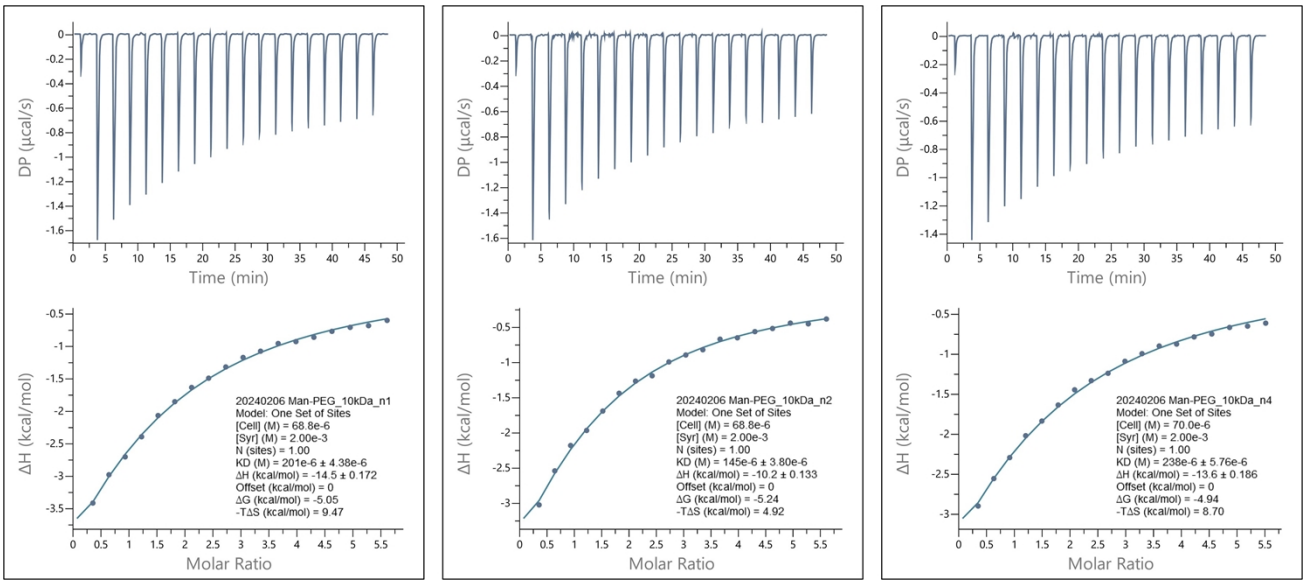

Figure S23. ITC data for the binding of **M1-PEG$_{10k}$-M1** to ConA at 25 ˚C. Raw thermograms after subtracting the control experiment at the top and binding isotherm (normalized heats versus molar ratio) at the bottom.

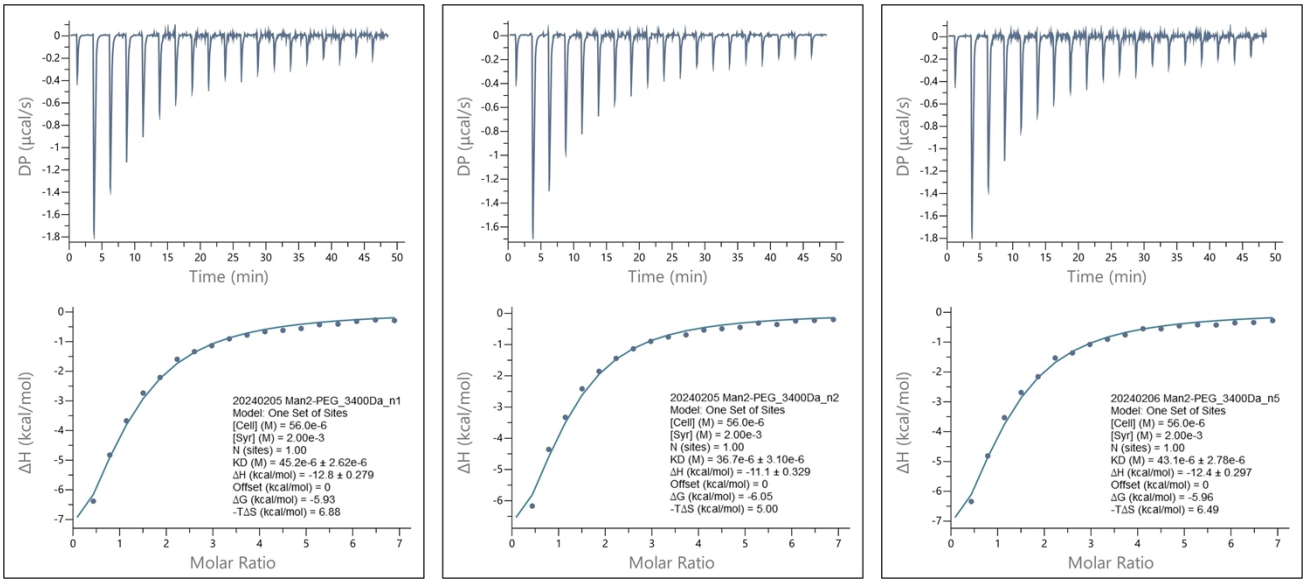

Figure S24. ITC data for the binding of **M2-PEG$_{3.4k}$-M2** to ConA at 25 ˚C. Raw thermograms after subtracting the control experiment at the top and binding isotherm (normalized heats versus molar

ratio) at the bottom.

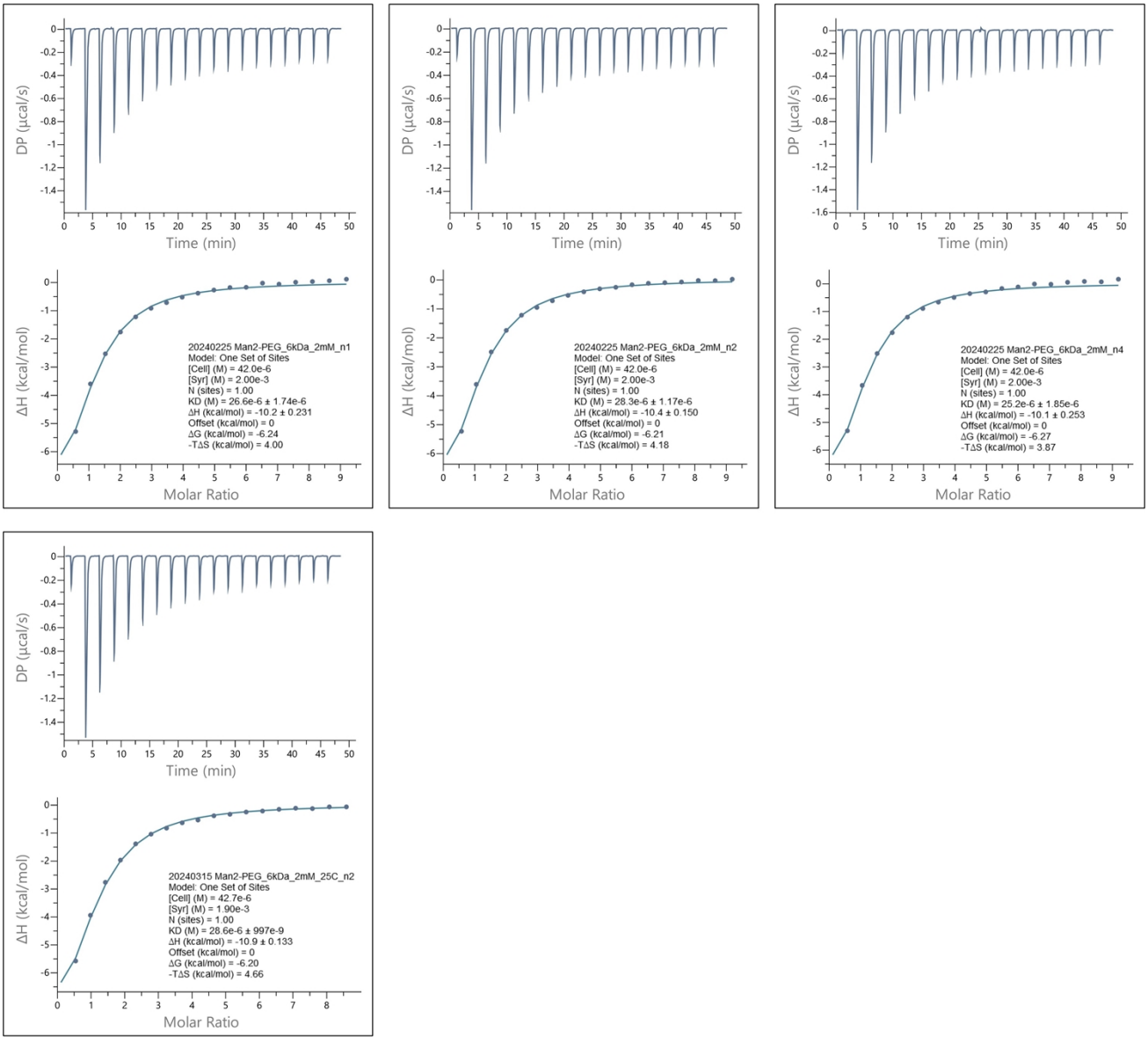

Figure S25. ITC data for the binding of **M2-PEG$_{6k}$-M2** to ConA at 25 ˚C. Raw thermograms after subtracting the control experiment at the top and binding isotherm (normalized heats versus molar ratio) at the bottom.

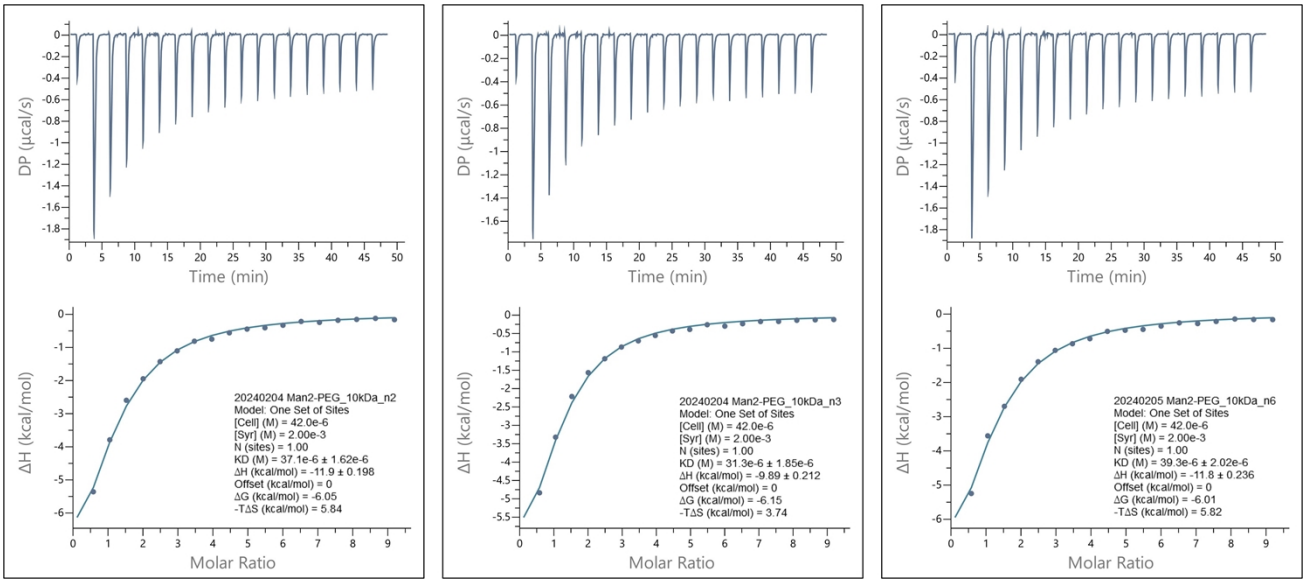

Figure S26. ITC data for the binding of **M2-PEG$_{10k}$-M2** to ConA at 25 ˚C. Raw thermograms after subtracting the control experiment at the top and binding isotherm (normalized heats versus molar ratio) at the bottom.

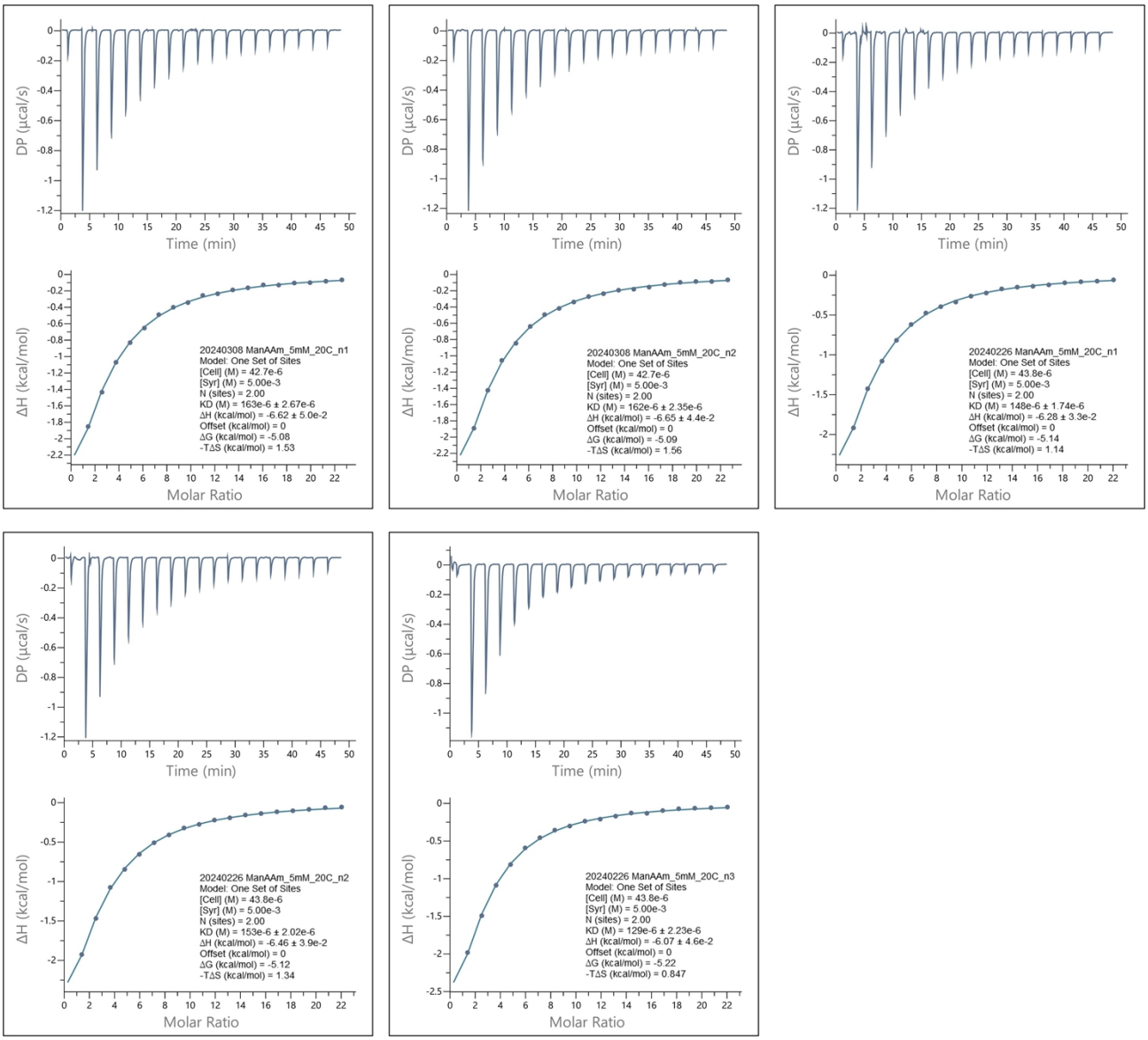

Figure S27. ITC data for the binding of ManAAm to ConA at 20 ˚C. Raw thermograms after subtracting the control experiment at the top and binding isotherm (normalized heats versus molar ratio) at the bottom.

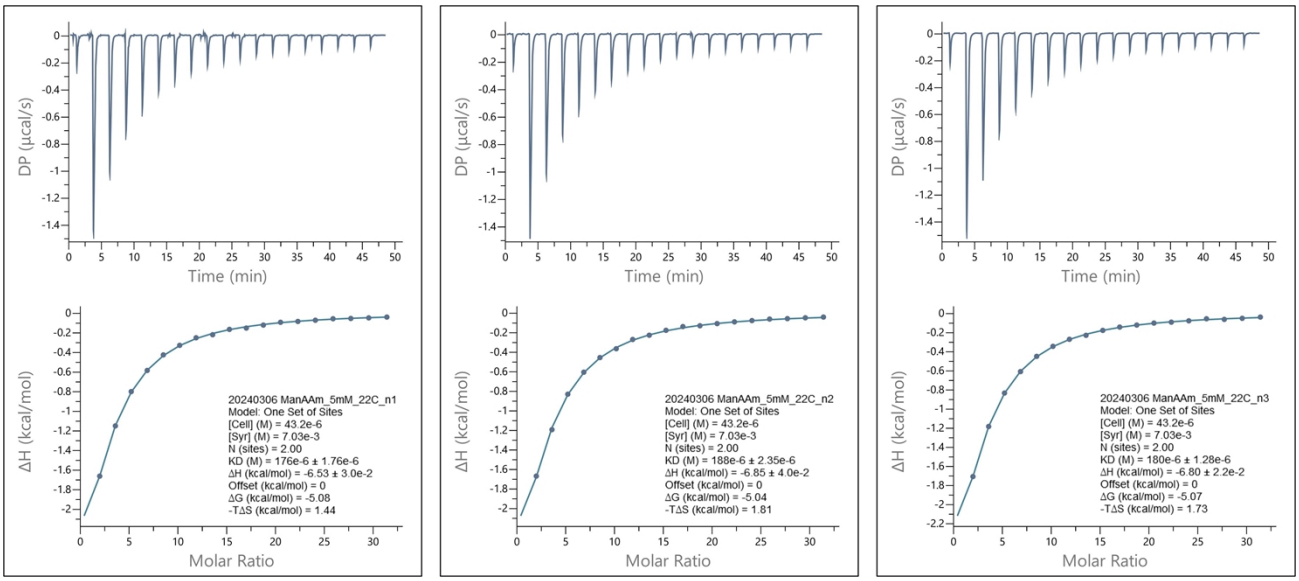

Figure S28. ITC data for the binding of ManAAm to ConA at 22.5 ˚C. Raw thermograms after subtracting the control experiment at the top and binding isotherm (normalized heats versus molar ratio) at the bottom.

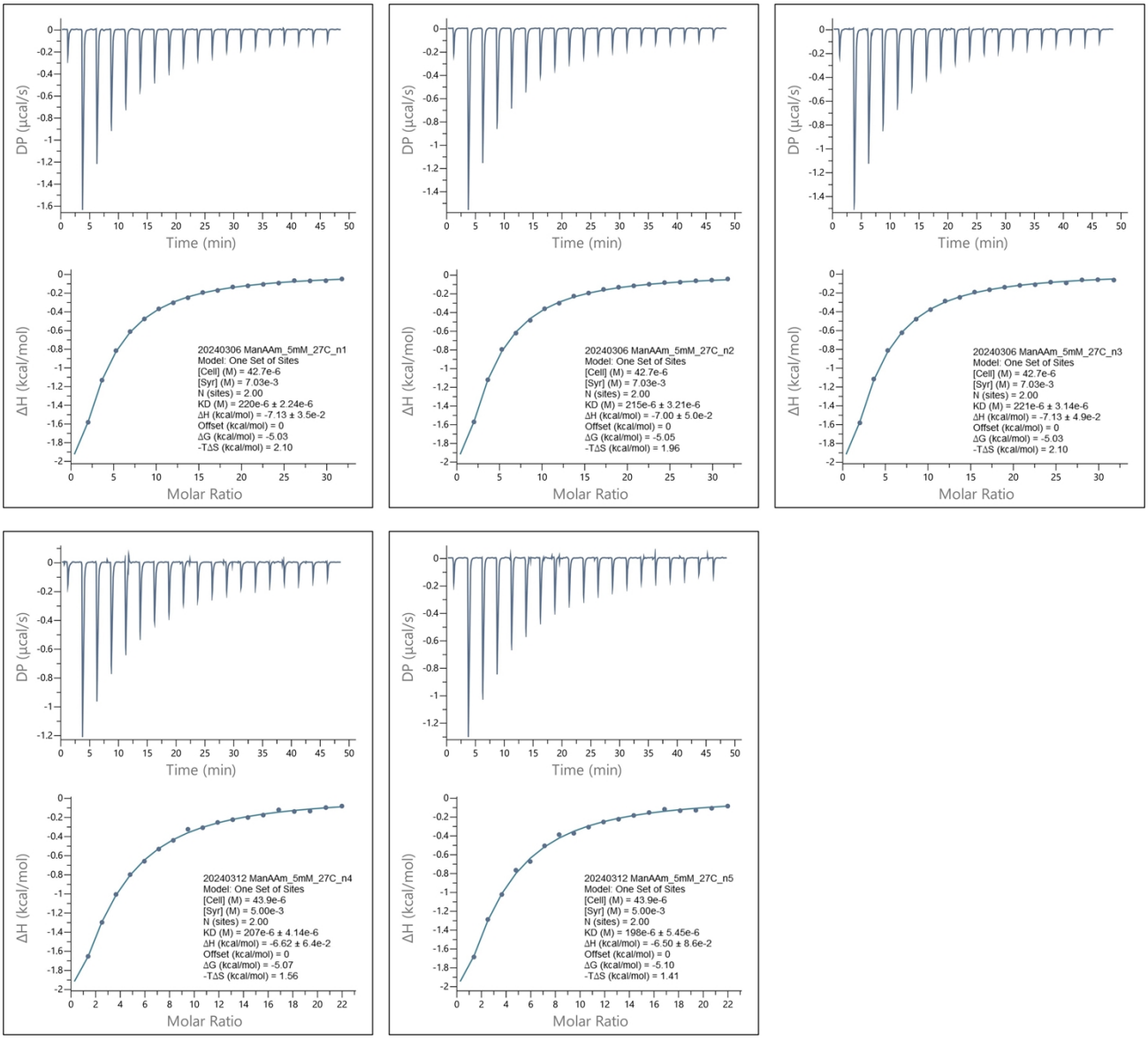

Figure S29. ITC data for the binding of ManAAm to ConA at 27.5 ˚C. Raw thermograms after subtracting the control experiment at the top and binding isotherm (normalized heats versus molar ratio) at the bottom.

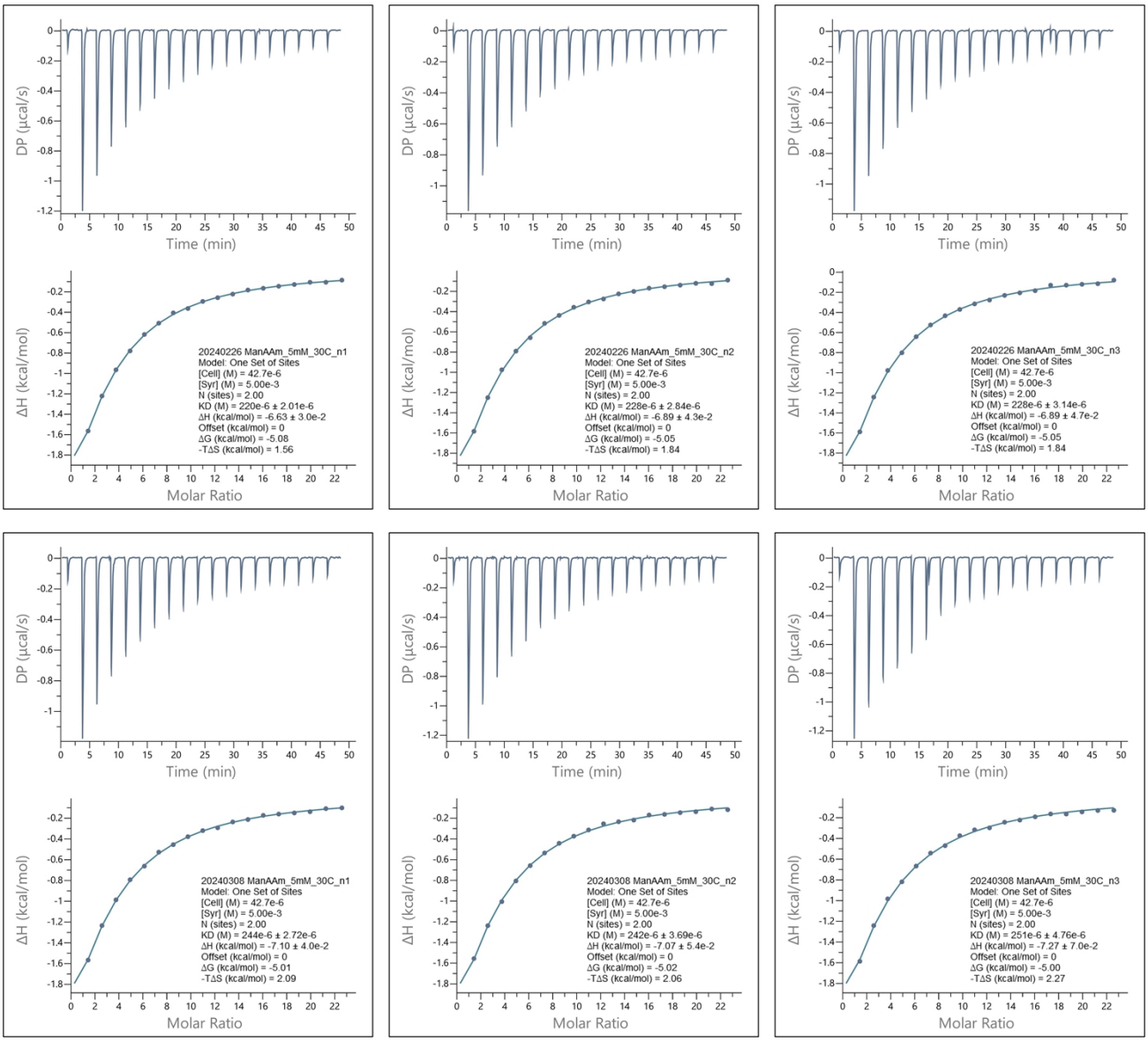

Figure S30. ITC data for the binding of ManAAm to ConA at 30 ˚C. Raw thermograms after subtracting the control experiment at the top and binding isotherm (normalized heats versus molar ratio) at the bottom.

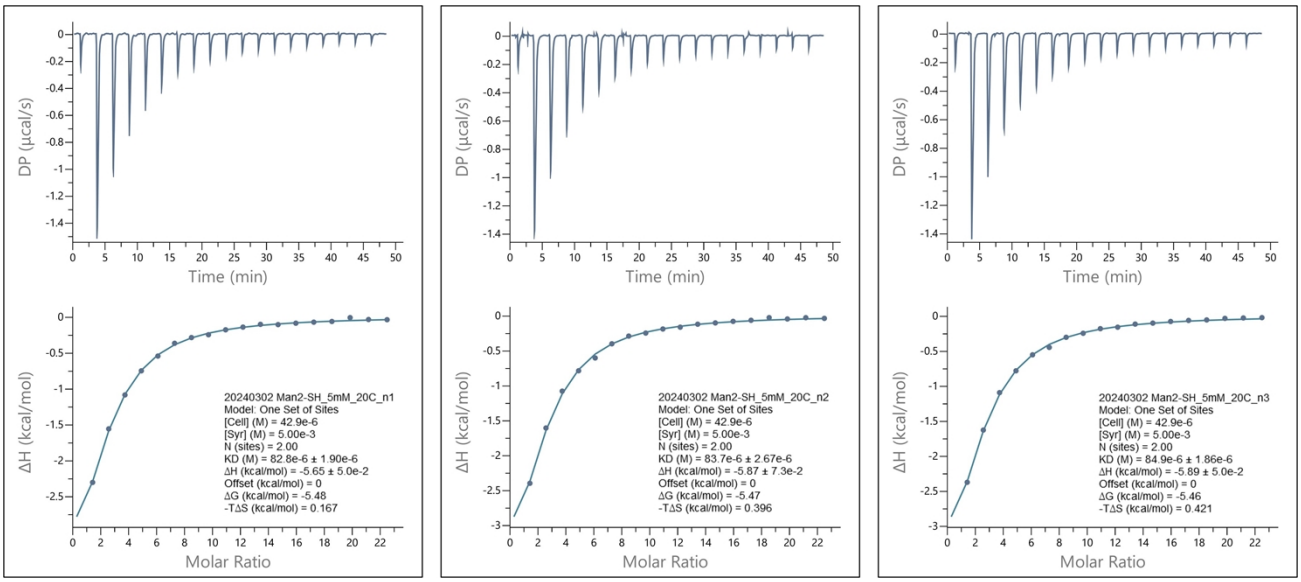

Figure S31. ITC data for the binding of **M2-SH** to ConA at 20 ˚C. Raw thermograms after subtracting the control experiment at the top and binding isotherm (normalized heats versus molar ratio) at the bottom.

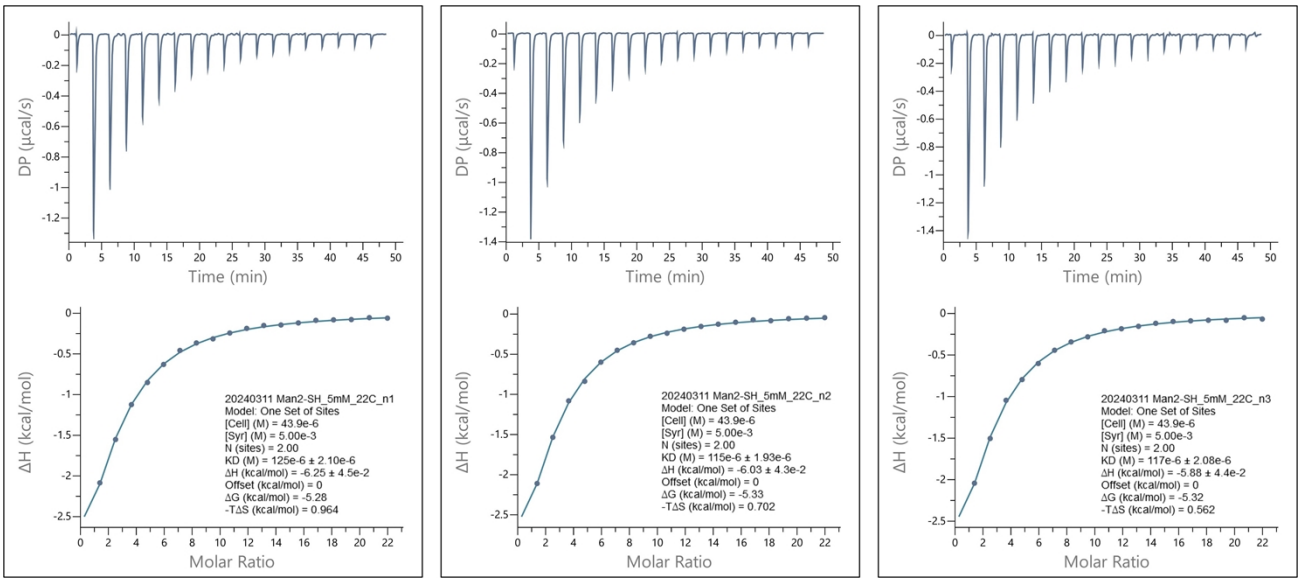

Figure S32. ITC data for the binding of **M2-SH** to ConA at 22.5 ˚C. Raw thermograms after subtracting the control experiment at the top and binding isotherm (normalized heats versus molar ratio) at the bottom.

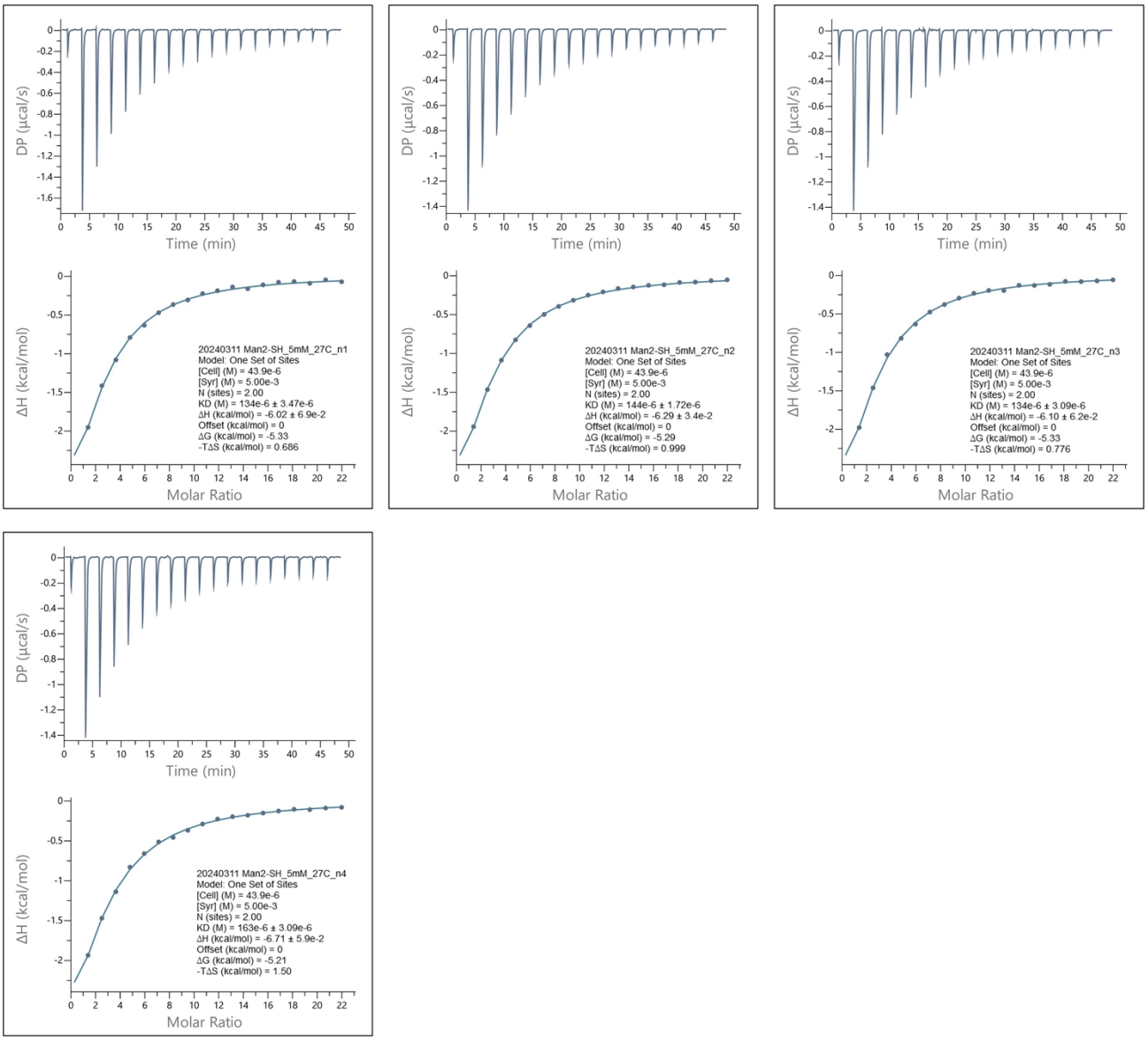

Figure S33. ITC data for the binding of **M2-SH** to ConA at 27.5 ˚C. Raw thermograms after subtracting the control experiment at the top and binding isotherm (normalized heats versus molar ratio) at the bottom.

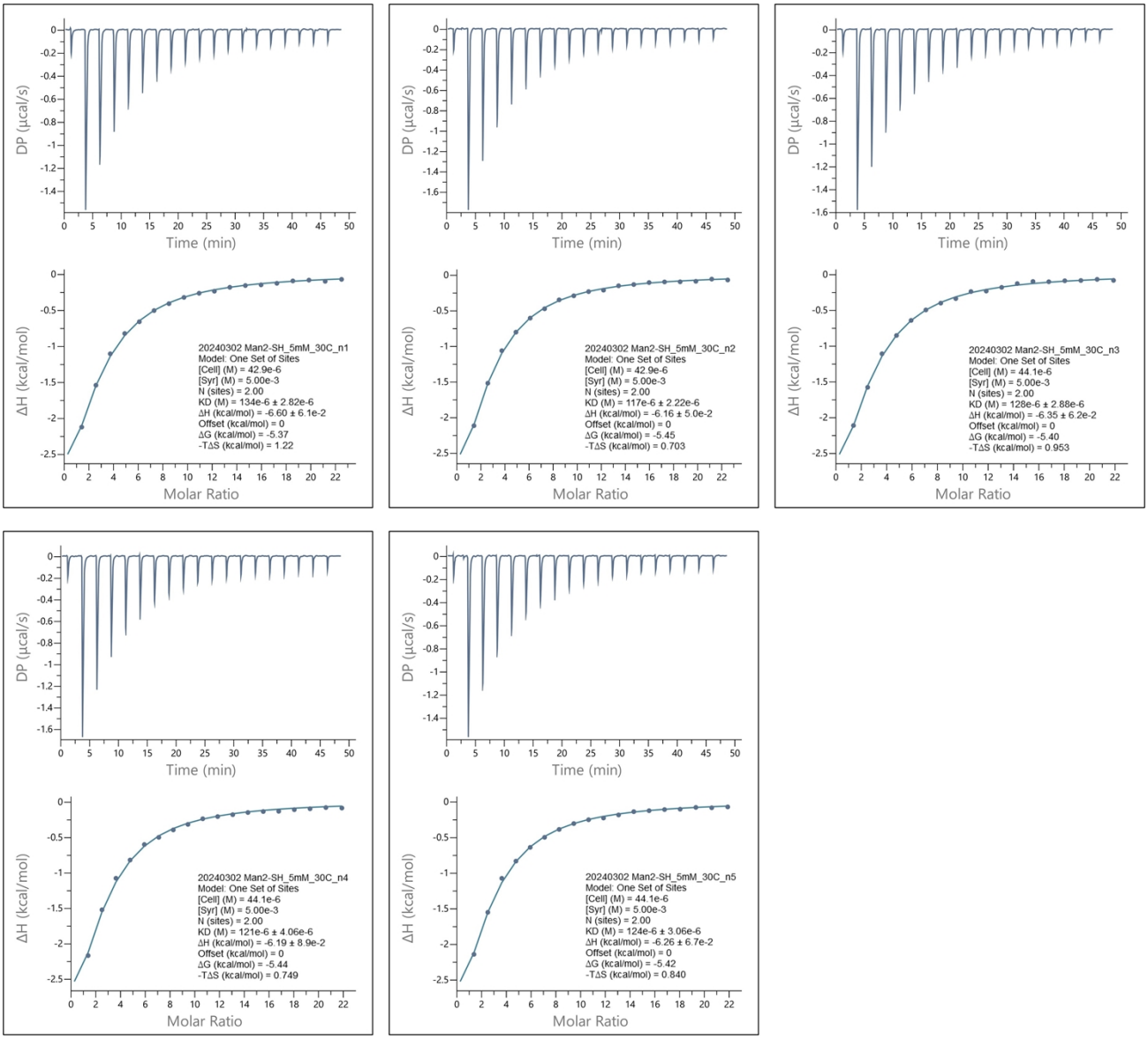

Figure S34. ITC data for the binding of **M2-SH** to ConA at 30 ˚C. Raw thermograms after subtracting the control experiment at the top and binding isotherm (normalized heats versus molar ratio) at the bottom.

Reference:

(1) M. Nagao, M. Kichize, Y. Hoshino, and Y. Miura, *Biomacromolecules* **2021**, *22*, 3119–3127.

(2) M. Nagao, Y. Hoshino, and Y. Miura, *J. Polym. Sci., Part A: Polm. Chem.* **2019**, *57*, 857–861.

(3) T. Banerjee, and N. Kishore, *J. Phys. Chem. B* **2006**, *110*, 7022–7028.